Title

Oligopeptide transporter Slc15A modulates macropinocytosis in Dictyostelium by maintaining intracellular nutrient status

Journal

Journal of Cell Science, 135(7)

ISSN

0021-9533

Authors

Zhang, Yiwei
Tu, Hui
Hao, Yazhou
et al.

Publication Date

2022-04-01

DOI

10.1242/jcs.259450

Peer reviewed

Oligopeptide transporter Slc15A modulates macropinocytosis in *Dictyostelium* by maintaining intracellular nutrient status

Yiwei Zhang[1,2,#], Hui Tu[1,2,#], Yazhou Hao[1,2], Dong Li[1,3], Yihong Yang[1], Ye Yuan[1,2], Zhonglong Guo[4], Lei Li[4], Haibin Wang[1,*], Huaqing Cai[1,2,*]

[1] National Laboratory of Biomacromolecules, Institute of Biophysics, Chinese Academy of Sciences, Beijing 100101, China

[2] College of Life Sciences, University of Chinese Academy of Sciences, Beijing 100049, China

[3] School of Life Sciences, University of Science and Technology of China, Hefei 230027, China

[4] State Key Laboratory of Protein and Plant Gene Research, School of Life Sciences and School of Advanced Agricultural Sciences, Peking University, Beijing 100871, China

[#] Yiwei Zhang and Hui Tu contributed equally to this work.

*Correspondence: Huaqing Cai (huaqingcai@ibp.ac.cn) and Haibin Wang (wanghaibin@ibp.ac.cn)

Abstract

Macropinocytosis mediates non-selective bulk uptake of extracellular fluid. It is the major route by which axenic *Dictyostelium* cells obtain nutrients and has emerged as a nutrient-scavenging pathway for mammalian cells. How environmental and cellular nutrient status modulates macropinocytic activity is not well understood. By developing a high-content imaging-based genetic screen in *Dictyostelium*, we identified Slc15A, an oligopeptide transporter localized at the plasma membrane and early macropinosome, as a novel macropinocytosis regulator. We show that deletion of *slc15A*, but not two other related *slc15* genes, leads to reduced macropinocytosis, slower cell growth, and aberrantly increased autophagy in cells grown in nutrient-rich medium. Expression of Slc15A or supplying cells with free amino acids rescues

these defects. In contrast, expression of transport-defective Slc15A or supplying cells with amino acids in their di-peptide forms fails to rescue these defects. Therefore, Slc15A modulates the level of macropinocytosis by maintaining the intracellular availability of key amino acids via oligopeptide extraction from the early macropinocytic pathway. We propose that Slc15A constitutes part of a positive feedback mechanism coupling cellular nutrient status and macropinocytosis.

Introduction

Macropinocytosis is a cellular process that mediates non-selective bulk uptake of extracellular fluid. Studies in the model system *Dictyostelium discoideum* and immune cells have greatly facilitated our understanding of the cellular mechanisms governing macropinocytosis (King and Kay, 2019). During this process, sheet-like extensions of the plasma membrane give rise to micrometer-sized vesicles called macropinosomes. In the initial step of macropinosome formation, membrane extensions evolve into macropinocytic cups, which are organized around patches of active Ras, Rac, and PIP_3, with actin polymerizing activities driven by the Scar/WAVE complex and formin proteins at the periphery and base of the patches, respectively (Buckley et al., 2020; Fujii et al., 2013; Junemann et al., 2016; Mylvaganam et al., 2021; Veltman et al., 2016; Yoshida et al., 2009). A tent pole mechanism in which filopodia-like F-actin extensions twist to constrict the forming macropinosomes has also been proposed (Condon et al., 2018). Once formed, macropinosomes can recycle to the cell surface or mature by trafficking through the endolysosomal system, where their contents are digested and extracted (Buckley and King, 2017; Donaldson, 2019; Freeman et al., 2020).

Macropinocytosis was originally recognized as a means for cells of the innate immune system, such as macrophages and dendritic cells, to survey environmental antigens for presentation to B cells and T cells (Lin et al., 2020; Norbury et al., 1995; Sallusto et al., 1995). More recently, studies in mammalian and *Dictyostelium* cells have uncovered an important metabolic function

of macropinocytosis (Charpentier et al., 2020; King and Kay, 2019; Palm, 2019). Various types of cancer cells exploit macropinocytosis to survive in nutrient-poor environments by ingesting extracellular macromolecules and breaking them down in the lysosome to fuel cell growth (Commisso et al., 2013; Kim et al., 2018; Palm et al., 2017; Palm et al., 2015; Ramirez et al., 2019; Wyant et al., 2017; Yao et al., 2019). Axenic laboratory strains of *Dictyostelium* utilize macropinocytosis to obtain nutrients, including glucose and amino acids, from liquid medium (Bloomfield et al., 2015; Williams and Kay, 2018). These strains were isolated that performed macropinocytosis at a high rate in liquid culture. The mutations that allow axenic growth have been mapped to three separate loci, one of which is a gene that encodes the RasGAP Neurofibromin (Bloomfield et al., 2015; Clarke and Kayman, 1987).

As a means of acquiring nutrients, the level of macropinocytosis is intrinsically connected to the cellular nutritional status. In pancreatic ductal adenocarcinoma (PDAC) tumor cells, glutamine deprivation or restricting extracellular proteins as the source of essential amino acids induces macropinocytosis (King et al., 2020; Lee et al., 2019). Amino acid shortage has also been shown to promote macropinocytosis in human placental trophoblasts (Shao et al., 2021). In axenic *Dictyostelium* cells, the presence of bacteria as a nutrient source promotes phagocytosis and suppresses macropinocytosis; switching the feeding strategy to liquid medium prominently increases the rate of macropinocytosis (Kayman and Clarke, 1983; Williams and Kay, 2018). Though these observations demonstrate that cells can calibrate their macropinocytic activity according to changes in nutrient conditions, how this is achieved in cells and the full complement of regulators remain to be elucidated.

We developed a forward genetic screen in *Dictyostelium* to seek novel macropinocytosis regulators. In this study, we characterized one of the genes isolated from the screen, which encodes an oligopeptide transporter we named Slc15A. We show that, opposite to the strategy in mammalian cells, Slc15A constitutes part of a positive feedback mechanism coupling cellular

nutrient status and macropinocytosis. Furthermore, Slc15A modulates the level of macropinocytosis by acting in the early macropinocytic pathway instead of the lysosome where nutrient extraction is thought to take place in canonical models. These results demonstrate that macropinocytosis and its regulation are far more sophisticated than we currently understand.

Results

Screening for macropinocytosis regulators identified Slc15A

To screen for macropinocytosis regulators, we generated a pool of restriction enzyme-mediated insertion (REMI) mutants in the axenic strain Ax2. Individual mutant clones were incubated with 70 kDa tetramethylrhodamine isothiocyanate dextran (TRITC dextran, TD) in liquid growth medium and then subjected to image-based high-content analysis (Fig. 1A). Cell boundaries and intracellular vesicles containing TD were identified in the digital phase contrast channel and fluorescent channel, respectively (Fig. 1A). The ratio of the total intensity of TD spots to the sum of cell area was used to quantify the activity of macropinocytosis. In addition to Ax2 cells, cells deleted of the class-1 PI3-kinases were used as controls. Consistent with previous reports (Hoeller et al., 2013), the *pi3k* deletion cells exhibited significantly reduced macropinocytosis under these experimental conditions (Fig. 1B).

From the screen, we obtained a series of macropinocytosis mutants (Fig. 1C). This report focuses on the gene (gene ID: DDB_G0272550) we named *slc15A*, which encodes a protein homologous to the mammalian solute carrier family 15 proteins (Fig. S1A). SLC15 proteins are proton-coupled oligopeptide transporters (POTs) mediating the cellular uptake of a wide range of di- and tri-peptides and peptide-like drugs (Daniel et al., 2006; Smith et al., 2013). Phylogenetic analysis revealed that the SLC15 family in eukaryotes constitutes two clades and *Dictyostelium* Slc15A is closely related to SLC15A1 and SLC15A2 in mammals (Fig. S1A). Sequence alignment showed that Slc15A shares 45-46% similarity to human SLC15A1 and SLC15A2 (Fig. S1B).

The REMI insertion site was identified at position 795 of the *slc15A* genomic locus (numbered from the ATG translation start site, Fig. S1B). To confirm that this insertion was responsible for the observed phenotype, we generated *slc15A* knockout (*slc15A*$^-$) cell line in Ax2 (Fig. S2A). The knockout cells exhibited similar phenotypes as the REMI mutant. When incubated with TD, substantially fewer and less bright TD-containing vesicles were observed in *slc15A*$^-$ cells compared to Ax2 cells (Fig. 2A,B). Similarly, the macropinocytic uptake of 70 kDa fluorescein isothiocyanate-dextran (FITC dextran, FD) was significantly impaired in *slc15A*$^-$ cells (Fig. S2B). Quantification of macropinocytosis over time corroborated these findings. The rate of macropinocytosis and the steady-state plateau were reduced by about 50% in *slc15A*$^-$ cells compared to the control (Fig. 2C). In contrast, fluid-phase exocytosis was not affected (Fig. 2D). Furthermore, the macropinocytosis defects associated with *slc15A* deletion could be fully rescued by expression of GFP- or RFP-tagged Slc15A (Fig. 2A-C, Fig. S2B). We also generated *slc15A*$^-$ cell line in the non-axenic strain DdB (Fig. S2C). Macropinocytic activity was considerably lower in DdB compared to Ax2 (Fig. S2D), and deletion of *slc15A* further decreased this activity (Fig. 2E,F). These experiments confirm that Slc15A is a novel regulator of macropinocytosis.

Slc15A is specifically required for macropinocytosis regulation

To begin elucidating the function of Slc15A, we examined the distribution and dynamics of several macropinocytic marker proteins in Ax2 and *slc15A*$^-$ cells. Rab5A, Rab7A, the V-ATPase subunit VatB, PIP_3/$PI(3,4)P_2$ sensor PHcrac, $PI(3,4)P_2$ sensor TAPP1, and PI(3)P sensor 2×FYVE were fused with GFP or RFP and used to mark macropinosomes at different stages (Buckley and King, 2017; Dormann et al., 2004; Egami et al., 2014; Maekawa et al., 2014; Rupper et al., 2001; Swanson, 2014). We observed that the overall organization of the macropinocytic pathway appeared unaffected by *slc15A* deletion. Marker proteins exhibited similar localization in Ax2 and *slc15A*$^-$ cells (Fig. 3A) and the sequential accumulation of PIP_3, $PI(3,4)P_2$, and PI(3)P proceeded with similar kinetics (Fig. 3B, Fig. S3). Measurement of macropinosome acidification also revealed no apparent defect in *slc15A*$^-$ cells (Fig. S4).

However, time-lapse imaging and quantification using PHcrac-GFP to mark macropinocytic cups and newly internalized macropinosomes revealed a significant reduction in the rate of macropinosome formation in *slc15A*$^{-}$ cells. Despite the production of similar-sized vesicles, the number of macropinosomes successfully generated per cell per minute was reduced by ~40% in *slc15A*$^{-}$ compared to Ax2 cells (Fig. 4A-C, Movie 1). In many instances, macropinocytic cups formed in *slc15A*$^{-}$ cells collapsed and receded to the plasma membrane without vesicle formation (Fig. 4A).

As macropinocytosis is the main pathway by which axenic cells obtain nutrients from liquid medium (Hacker et al., 1997), its defect often manifests as slow cell growth. Indeed, the generation time in shaken suspension increased from ~8 h for Ax2 cells to ~15 h for *slc15A*$^{-}$ cells (Fig. 4D). Expression of Slc15A-GFP rescued this defect (Fig. 4D). Lack of nutrient uptake has also been shown to upregulate autophagy. Imaging the autophagy marker GFP-Atg8a (King et al., 2011) revealed that, although non-nutrient development buffer (DB) induced autophagy to a similar extent in Ax2 and *slc15A*$^{-}$ cells, the latter showed significantly increased autophagy in the commonly used HL5 growth medium (Fig. 4E,F; Movies 2-3). The increase of Atg8a structures in *slc15A*$^{-}$ cells was not caused by a block of autophagy flux (Fig. S5). Therefore, *slc15A* deletion likely impairs macropinocytosis-mediated nutrient uptake, resulting in reduced cell growth and aberrantly increased autophagy in cells cultured in nutrient-rich medium.

In addition to liquid medium, *Dictyostelium* cells could utilize bacteria as the nutrient source through phagocytosis. We investigated whether Slc15A is involved in the regulation of phagocytosis. When plated on bacterial (*Klebsiella aerogenes*) lawns, the plaque growth of *slc15A*$^{-}$ cells was indistinguishable from that of Ax2 cells, indicating that bacterial uptake and digestion were not affected (Fig. S2A). Quantifying bacteria phagocytosis via flow cytometry analysis and assaying the proteolytic activity of bacteria-containing phagosomes confirmed this conclusion (Fig. 4G,H). Together, these experiments indicate that Slc15A is specifically involved in the regulation of macropinocytic, but not phagocytic, growth.

Slc15A promotes macropinocytosis by maintaining intracellular availability of amino acids

To determine whether Slc15A modulates macropinocytosis via its putative function as an oligopeptide transporter, we generated Slc15A bearing mutations (Slc15A^{mut}-GFP) in the two conserved residues, R68 and E438 (Fig. S1B). The corresponding mutations, R57H in human SLC15A2 and E595R in SLC15A1, were shown to abolish transport function (Terada et al., 2004; Xu et al., 2009). Slc15A^{mut}-GFP was expressed at a similar level as its WT counterpart. However, it failed to rescue the defects in TD uptake and cell growth (Fig. 5A-C), suggesting that the oligopeptide transport activity is required for Slc15A to regulate macropinocytosis.

The standard HL5 medium contains amino acids, peptides, and proteins derived from peptone and yeast extract. We speculated that deletion of *slc15A* may cause reduced peptide import from HL5 and thus a lack of amino acid-nutrients in cells, which may in turn downregulate macropinocytosis. If this were true, providing *slc15A*$^{-}$ cells with free amino acids, which bypass the need for peptide transport, should rescue the macropinocytosis defects. To test this, we switched out the HL5 medium for SIH medium, a synthetic medium containing a defined composition of free amino acids sufficient for sustaining cell growth. Growing *slc15A*$^{-}$ cells in SIH medium fully rescued the macropinocytosis defect (Fig. 5D,E; Fig. S6). Cell growth and autophagy regulation were also restored (Fig. 5F,G; Movies 2-3). These experiments support the hypothesis that reduced amino acid availability underlies the macropinocytosis defect of *slc15A*$^{-}$ cells.

To determine whether specific amino acids within the SIH medium are crucial for the rescuing effect, we subjected *slc15A*$^{-}$ cells to SIH medium lacking arginine, glutamate, or lysine. The three amino acids were shown to be needed for the upregulation of macropinocytosis when the feeding strategy was switched from growth on bacteria to liquid medium (Williams and Kay, 2018). Intriguingly, removing arginine (SIH-R) or lysine (SIH-K), but not glutamate (SIH-E), abolished the ability of SIH medium to rescue the macropinocytosis defect caused by *slc15A*

deletion (Fig. 6A,B). Ax2 cells cultured in SIH-R or SIH-K also exhibited reduced macropinocytosis (Fig. 6A,B). These results indicate that *slc15A* deletion likely causes reduced availability of key amino acids including arginine and lysine.

To further test that Slc15A-mediated oligopeptide transport contributes to the intracellular pool of arginine and lysine, we subjected cells to medium containing synthesized dipeptide of arginine (R-R) or lysine (K-K). Supplementing R-R or K-K restored the macropinocytosis ability of Ax2 cells grown in SIH-R or SIH-K. However, it failed to do so for *slc15A*$^{-}$ cells, confirming that the knockout cells are defective in dipeptide utilization (Fig. 6C,D). These experiments collectively indicate that Slc15A promotes macropinocytosis by functioning as an oligopeptide transporter to maintain the intracellular availability of key amino acids.

Slc15A functions in the early macropinocytic pathway

Extracellular proteins taken up by macropinocytosis are thought to be delivered to the lysosomes, degraded into amino acids, and then exported to the cytosol to fuel metabolism (Verdon et al., 2017; Wyant et al., 2017). However, we noticed that Slc15A did not appear to localize on lysosomal vesicles when expressed from extrachromosomal plasmids. To determine the localization more accurately, we generated Slc15A-GFP and Slc15A-RFP knock-in (KI) cells (Fig. S2E). We found that Slc15A localized at the plasma membrane in these cells and, when the membrane deformed to produce macropinosomes, remained associated with newly generated macropinosomes (Fig. 7A,B). Imaging Slc15A together with TAPP1 and 2×FYVE revealed that Slc15A and TAPP1 colocalized on macropinosomes during cup closure and initial trafficking (Fig. 7A, Movie 4); the signal of Slc15A gradually decreased as the macropinosomes moved further into the cells, which was accompanied by the gradual accumulation of 2×FYVE (Fig. 7B). These experiments indicate that Slc15A recycles from the macropinosomes in the early stages of the pathway. In line with this finding, we found little overlap between Slc15A and the lysosomal/postlysosomal marker LmpA (Sattler et al., 2018) (Fig. S7). Thus, Slc15A likely

mediates oligopeptide transport across the plasma membrane or the early macropinosomal membrane but not efflux from the lysosome.

Given that the SLC15 family proteins rely on an electrochemical H^+ gradient for transport activity (Smith et al., 2013; Steel et al., 1997), we examined whether the presence of Slc15A on nascent macropinosomes overlapped with macropinosome acidification. By incubating Slc15A-RFP KI cells with FD, we found that newly generated macropinosomes quickly acquired an acidic environment indicated by the decrease of the fluorescence of FD before Slc15A-RFP was evidently recycled (Fig. 7C). Quantification revealed that Slc15A associated with newly internalized macropinosome for 115 ± 31 sec (from 15 macropinosomes), whereas macropinosome acidification was initiated almost immediately after cup closure with a significant change occurring within 60 sec (Fig. S4). Imaging Slc15A together with VatB also revealed that the recruitment of V-ATPase to macropinosomes started before the recycling of Slc15A (Fig. 7D). We speculate that the rapid acidification of nascent macropinosomes may facilitate the function of Slc15A by providing a steeper proton gradient. However, at this stage we cannot rule out the possibility that Slc15A also functions at the plasma membrane.

Discussion

In summary, we identified Slc15A as a macropinocytosis-specific regulator. We demonstrate that Slc15A is not directly involved in macropinosome formation or maturation; instead, it sustains the macropinocytic activity of cells by mediating oligopeptide transport from growth medium and maintaining the intracellular availability of key amino acids (Fig. 8). The *Dictyostelium* genome encodes two other putative SLC15 family proteins (Fig. S1A). However, these two proteins did not localize to the macropinocytic pathway and their disruption did not affect macropinocytosis (Fig. S8), confirming a unique function of Slc15A.

Characterization of Slc15A allowed us to gain fresh insights into macropinocytosis regulation. First, the localization study suggested that Slc15A functions earlier in the macropinocytic pathway. Thus, different from the canonical model, the lysosome is not the only cellular compartment where nutrients internalized are extracted. Although it is not yet feasible to pinpoint precisely where Slc15A-mediated transport occurs, we speculate that nascent macropinosomes are the more probable compartments, because their acidic environment could promote the function of Slc15A. The characteristic substrate multispecificity of SLC15 proteins may further facilitate nutrient extraction in the form of oligopeptides before reaching lysosome (Ito et al., 2013). Intriguingly, the defects in *slc15A*$^{-}$ cells were alleviated by feeding cells with free amino acids, which may be delivered to the cell via amino acid transporters. This ability to retrieve nutrients in different forms and possibly at different stages along the macropinocytic pathway likely promotes metabolic flexibility.

Second, our study indicates that Slc15A contributes to a positive feedback mechanism coupling cellular nutrient status and macropinocytosis (Fig. 8). Disrupting Slc15A or depleting arginine or lysine from the growth medium all led to reduced macropinocytosis. Combined with previous studies analyzing macropinocytosis during feeding strategy switch (Williams and Kay, 2018), these experiments convincingly demonstrate that the intracellular availability of key amino acids can, in turn, promote the macropinocytic activity of *Dictyostelium* cells, constituting feedback regulation. Interestingly, seemingly opposite strategies are taken by *Dictyostelium* and mammalian cells to cope with amino acid stress conditions; *Dictyostelium* cells downregulate macropinocytosis, whereas mammalian cells upregulate the process (Lee et al., 2019; Shao et al., 2021). Such a difference may reflect different survival strategies. Starvation in *Dictyostelium* ultimately leads to multicellular development, a process that benefits from reduced macropinocytosis (Veltman et al., 2014; Veltman et al., 2016), whereas mammalian cells lacking this alternative route may instead resort to macropinocytosis upregulation and protein-scavenging.

Future studies are needed to elucidate how intracellular nutrient levels are sensed and transduced to regulate macropinocytosis in *Dictyostelium*. In other systems, amino acid-sensing is mediated by activation of the mechanistic target of rapamycin complex 1 (mTORC1) pathway (Wolfson and Sabatini, 2017). It is possible that mTORC1 senses the nutrient stress condition in *slc15A*$^{-}$ cells to downregulate macropinocytosis. However, pharmacological inhibition of mTORC1 or depletion of the mTORC1-specific component Raptor does not affect macropinocytosis in *Dictyostelium* (Rosel et al., 2012; Williams and Kay, 2018), suggesting that the feedback regulation likely involves yet unidentified pathways. Additionally, as SLC15 orthologues exist throughout the eukaryotic kingdom, it will also be of great interest to investigate whether this family of proteins is involved in the regulation of macropinocytosis in other species.

Materials and Methods

Cell growth

Ax2 cells were used as the axenic strain and were routinely cultured in HL5 medium (Formedium, HLF3). Cells carrying expression constructs were maintained in HL5 containing G418 (10-20 µg/ml) or hygromycin (50-100 µg/ml). Development buffer (DB) contained 5 mM Na_2HPO_4, 5 mM KH_2PO_4, 2 mM $MgSO_4$, and 0.2 mM $CaCl_2$. Growth rate was measured by seeding cells at $0.5x10^5$/mL and counting cell density for 4 consecutive days. DdB cells were used the non-axenic wild-type strain. Non-axenic cells were cultured in SorMC buffer (15 mM KH_2PO_4, 2mM Na_2HPO_4, 50 µM $MgCl_2$, 50 µM $CalCl_2$, pH 6.0) containing *K. aerogenes* (OD_{600} = 2) or grown on *K. aerogenes* lawns as described before (Paschke et al., 2018).

REMI screen

REMI mutants were generated as described previously (Kuspa, 2006; Shaulsky et al., 1996). In brief, DNA fragment containing a blasticidin resistant cassette (BSR) was digested with BamHI and co-transformed into cells with the DpnII restriction enzyme. Cells were dispensed into 96-well dishes in HL5 medium and blasticidin (10 µg/ml) was added the next day to select

mutant clones with BSR inserted into the genome. Individual mutant clones were seeded in 96-well plates in growth medium, incubated with 70 kDa TD (Sigma T1162) for 1 h, and then analyzed using a PerkinElmer Phenix Opera high-content screening system. Images were captured in the digital phase contrast channel and TRITC channel with nine fields per well using a 63 × water lens. Image analyses were performed using the built-in Harmony software. For gene identification of REMI mutants, genomic DNA was digested with PsiI and ligated to circularize fragments, and inverse PCR was performed using a pair of outward-facing primers located within the BSR sequence as described previously (Keim et al., 2004). The obtained PCR bands were then sequenced to identify the insertion sites.

Molecular biology

To make knockout constructs for *slc15A*, *slc15B*, and *slc15C* deletion in Ax2, a BSR cassette (Faix et al., 2004) was inserted into pBlue-Script II SK+ to generate pBlueScript-BSR. 5' and 3' arms were PCR-amplified from genomic DNA with primers listed in Table 1 and cloned upstream and downstream of the BSR cassette, respectively. The resulting disruption cassette was PCR amplified and electroporated into Ax2. Gene disruption was confirmed by resistance to blasticidin (10 µg/ml) and PCR amplification. To make knockout construct for *slc15A* deletion in DdB, 5' and 3' arms were PCR amplified with primers listed in Table 1 and cloned upstream and downstream of the NeoR cassette in pDM1082, respectively. Transfection and selection were performed as described before (Paschke et al., 2018). Gene disruption was confirmed by resistance to G418 (10 µg/ml) and PCR. Slc15A-GFP knock-in cell was generated by replacing the region of *slc15A* between +1920 and +1922 with a GFP-hygromycin cassette from pDM1355 (Paschke et al., 2018). GFP was replaced with RFP to generate the Slc15A-RFP knock-in cassette. Knock-in clones were selected by resistance to hygromycin and confirmed by PCR and Western Blotting.

To generate constructs expressing GFP- or RFP-fusion proteins, DNA fragments encoding *Dictyostelium* Slc15A, Slc15B, Slc15C, Atg8a, Rab5A, Rab7A, VatB, LmpA, and human TAPP1 were PCR-amplified using primers listed in Table 1 and cloned into *Dictyostelium* pDM expression vectors (Veltman et al., 2009) containing a multiple cloning site. To generate construct expressing GFP-2×FYVE, a fragment containing 2×FYVE domain of *C. elegans* EEA1 was released from a *C. elegans* expression vector (Li et al., 2009) and cloned into pDM317. To generate Slc15A$^{R68H/E438R}$-GFP, the arginine residue at position 68 and glutamic acid residue at position 438 were mutated to histidine and arginine, respectively. To generate constructs expressing RFP-GFP-Atg8a, *atg8a* was first cloned into pDM449 containing a multiple cloning site; GFP was then PCR amplified from pDM317 using primers listed in Table 1 and inserted in between RFP and Atg8a.

Macropinocytosis and exocytosis assays

Macropinocytosis assay by microscopy imaging was routinely performed by incubating cells with 500 ng/μL TD (Sigma T1162) in HL5 for 1 h. For experiments presented in figure 2E, bacterially grown non-axenic cells were adapted in HL5 medium supplemented with 10% fetal bovine serum (Gibco 10091-148) for 24 h before incubating with TD in fresh medium. For experiments presented in figure 6A, cells cultured in SIH medium (Formedium) were shifted to SIH-K/R/E for 48 h before measuring macropinocytosis. For experiments in figure 6C, cells cultured in SIH were shifted to SIH-R or SIH-K for 48 h, followed by the addition of R (87.5 mg/L), R-R dipeptide (87.5 mg/L), K (156 mg/L), or K-K dipeptide (156 mg/L) for 24 h before measuring macropinocytosis. To quantify TD uptake, the medial optical section of cell was imaged using a Zeiss 880 inverted microscope equipped with a 63 ×/1.4 oil immersion objective. Fluorescence intensity was quantified by ImageJ and normalized to cell area.

Macropinocytosis dynamics was recorded in Ax2 and *slc15A*$^{-}$ cells expressing PHcrac-GFP by time-lapse imaging. The rate of macropinocytosis was quantified by tracking the number of enclosed macropinosomes formed in 5 min. Macropinosome size was determined by measuring

the area of newly formed macropinosomes immediately after ruffle closure with the freehand line tool in ImageJ.

Fluorimetric analysis of macropinocytosis and exocytosis was performed as described before (Rivero and Maniak, 2006). For macropinocytosis measurement, cells were shaken at a density of 5×10^6/ml in growth medium, and TD was added to a final concentration of 1 mg/ml. Aliquots of 300 µl of cells were taken at each time point and mixed briefly with Trypan Blue solution (2 mg/ml in 20 mM citrate and 150 mM NaCl, pH 4.5) on ice. Cells were washed once with 1 ml ice-cold Sörensen buffer (14.6 mM KH_2PO_4, 2.0 mM Na_2HPO_4, pH 6.1) and resuspended in 0.5 ml Sörensen buffer. For exocytosis measurement, cells were first incubated with 1 mg/ml TD for 180 min, and were then washed and resuspended in fresh HL5 medium. Aliquots of 300 µl of cells were taken at each time point, washed, and resuspended in 0.5 ml ice-cold Sörensen buffer. In both experiments, fluorescence was measured immediately using a Tecan Spark fluorescence spectrophotometer (544-nm excitation and 574-nm emission). Obtained values were normalized to protein content.

Phagocytosis assays

Expression of mCherry or GST-GFP was induced in *E.coli* strain BL21 (DE3) with 0.3 mM isopropyl β-D-1-thiogalactoside at 16°C overnight. Harvested bacteria were washed with Sörensen buffer. For flow cytometry analysis, cells were shaken at a density of 4×10^6/ml in Sörensen buffer, and mCherry-expressing bacteria were added to a final density of 2×10^9/ml. Aliquots of 0.5 ml were taken at each time point. Cells were washed with ice-cold Sörensen buffer containing 5 mM sodium azide and resuspended in Sörensen buffer. The total fluorescence intensity per cell was determined by a BD Biosciences Influx flow cytometer and data was analyzed by FlowJo. For bacteria killing assay, GFP-expressing bacteria were resuspended in HL5 medium to a concentration 2×10^8/mL. 10 µl of bacteria culture in 400 µl HL5 was added into 8-well coverslip chamber before addition of 10^5 cells. Images were acquired every 14 sec for a total of 100 frames.

Imaging

All microscopy experiments were performed at 22°C. To image the localization of fluorescent proteins in cells, 10^5 cells were plated in an 8-well coverslip chamber (Lab-Tek; NalgenNunc) and allowed to adhere. Images were taken on a Zeiss 880 inverted microscope equipped with a 40 ×/0.95 or 63 ×/1.4 oil-immersion objective. To image Atg8a-GFP signal, cells were incubated in HL5 or submerged in DB for 1 h before imaging. For experiments presented in figure S5A, the HL5 medium was supplemented with 2.5 × protease inhibitor cocktail (Roche 11836170001) under the plus PIC condition.

For experiments presented in figure 7C, cells were plated in an 8-well coverslip chamber and allowed to adhere. Before imaging, the medium was replaced by fresh HL5 medium containing 1 mg/ml FD. For experiments presented in figure S4, cells were incubated in HL5 medium containing 1 mg/ml FD and 500 μg/ml TD. FD and TD signals contained within the newly generated macropinosomes were quantified by ImageJ. The ratio of FD to TD was used to measure macropinosome acidification with the maximum ratio normalized to 1.

Quantification and statistical analysis

SuperPlots were generated as described previously (Lord et al., 2020). Statistical analysis was performed using GraphPad Prism. In all figures, *** indicates $p < 0.001$, ** $p < 0.01$, and * $p < 0.05$.

Acknowledgments

We thank Dr. Robert Kay (MRC Laboratory of Molecular Biology, UK) for providing Ax2, DdB, *pi3k1-5*$^-$ cells and pDM vectors; Dr. Richard Firtel (University of California San Diego, US) for *pi3k1-2*$^-$ cells; Dr. Xiaochen Wang (Institute of Biophysics, Chinese Academy of Sciences, China) for FYVE and TAPP1 plasmids; and Dr. Jason King (University of Sheffield, UK) for RFP-VatB plasmid.

Funding

This work was supported by grants from the Ministry of Science and Technology of China (2021YFA1300301), the Strategic Priority Research Program of Chinese Academy of Sciences (XDB37020304), the National Natural Science Foundation of China (32170701, 32071232, and 31872828), and the Youth Innovation Promotion Association of Chinese Academy of Sciences (2020096).

Author contributions

H. Cai designed research; Y. Zhang, H. Tu, H. Wang, Y. Hao, D. Li, Y. Yang, and Y. Yuan performed research; H. Cai, Y. Zhang, H. Tu, H. Wang, Z. Guo, and L. Li analyzed data; and H. Cai, H. Wang, Y. Zhang, and H. Tu wrote the manuscript.

Competing interests

The authors declare no competing or financial interests.

Data availability

The authors declare that all data supporting the findings of this study are available within the paper and its supplementary information files.

References

Bloomfield, G., D. Traynor, S.P. Sander, D.M. Veltman, J.A. Pachebat, and R.R. Kay. 2015. Neurofibromin controls macropinocytosis and phagocytosis in Dictyostelium. *Elife*. 4.

Buckley, C.M., and J.S. King. 2017. Drinking problems: mechanisms of macropinosome formation and maturation. *Febs J*. 284:3778-3790.

Buckley, C.M., H. Pots, A. Gueho, J.H. Vines, C.J. Munn, B.A. Phillips, B. Gilsbach, D. Traynor, A. Nikolaev, T. Soldati, A.J. Parnell, A. Kortholt, and J.S. King. 2020. Coordinated Ras and Rac Activity Shapes Macropinocytic Cups and Enables Phagocytosis of Geometrically Diverse Bacteria. *Curr Biol*. 30:2912-2926 e2915.

Charpentier, J.C., D. Chen, P.E. Lapinski, J. Turner, I. Grigorova, J.A. Swanson, and P.D. King. 2020. Macropinocytosis drives T cell growth by sustaining the activation of mTORC1. *Nat Commun*. 11:180.

Clarke, M., and S.C. Kayman. 1987. The axenic mutations and endocytosis in Dictyostelium. *Methods in cell biology*. 28:157-176.

Commisso, C., S.M. Davidson, R.G. Soydaner-Azeloglu, S.J. Parker, J.J. Kamphorst, S. Hackett, E. Grabocka, M. Nofal, J.A. Drebin, C.B. Thompson, J.D. Rabinowitz, C.M. Metallo, M.G. Vander Heiden, and D. Bar-Sagi. 2013. Macropinocytosis of protein is an amino acid supply route in Ras-transformed cells. *Nature*. 497:633-+.

Condon, N.D., J.M. Heddleston, T.L. Chew, L. Luo, P.S. McPherson, M.S. Ioannou, L. Hodgson, J.L. Stow, and A.A. Wall. 2018. Macropinosome formation by tent pole ruffling in macrophages. *J Cell Biol*. 217:3873-3885.

Daniel, H., B. Spanier, G. Kottra, and D. Weitz. 2006. From bacteria to man: archaic proton-dependent peptide transporters at work. *Physiology*. 21:93-102.

Donaldson, J.G. 2019. Macropinosome formation, maturation and membrane recycling: lessons from clathrin-independent endosomal membrane systems. *Philosophical transactions of the Royal Society of London. Series B, Biological sciences*. 374:20180148.

Dormann, D., G. Weijer, S. Dowler, and C.J. Weijer. 2004. In vivo analysis of 3-phosphoinositide dynamics during Dictyostelium phagocytosis and chemotaxis. *J Cell Sci*. 117:6497-6509.

Egami, Y., T. Taguchi, M. Maekawa, H. Arai, and N. Araki. 2014. Small GTPases and phosphoinositides in the regulatory mechanisms of macropinosome formation and maturation. *Front Physiol*. 5:374.

Faix, J., L. Kreppel, G. Shaulsky, M. Schleicher, and A.R. Kimmel. 2004. A rapid and efficient method to generate multiple gene disruptions in Dictyostelium discoideum using a single selectable marker and the Cre-loxP system. *Nucleic acids research*. 32:e143.

Freeman, S.A., S. Uderhardt, A. Saric, R.F. Collins, C.M. Buckley, S. Mylvaganam, P. Boroumand, J. Plumb, R.N. Germain, D.J. Ren, and S. Grinstein. 2020. Lipid-gated monovalent ion fluxes regulate endocytic traffic and support immune surveillance. *Science*. 367:301-+.

Fujii, M., K. Kawai, Y. Egami, and N. Araki. 2013. Dissecting the roles of Rac1 activation and deactivation in macropinocytosis using microscopic photo-manipulation. *Scientific reports*. 3:2385.

Hacker, U., R. Albrecht, and M. Maniak. 1997. Fluid-phase uptake by macropinocytosis in Dictyostelium. *J Cell Sci*. 110 (Pt 2):105-112.

Hoeller, O., P. Bolourani, J. Clark, L.R. Stephens, P.T. Hawkins, O.D. Weiner, G. Weeks, and R.R. Kay. 2013. Two distinct functions for PI3-kinases in macropinocytosis. *J Cell Sci*. 126:4296-4307.

Junemann, A., V. Filic, M. Winterhoff, B. Nordholz, C. Litschko, H. Schwellenbach, T. Stephan, I. Weber, and J. Faix. 2016. A Diaphanous-related formin links Ras signaling directly to actin assembly in macropinocytosis and phagocytosis. *Proc Natl Acad Sci U S A*. 113:E7464-E7473.

Kayman, S.C., and M. Clarke. 1983. Relationship between axenic growth of Dictyostelium discoideum strains and their track morphology on substrates coated with gold particles. *J Cell Biol*. 97:1001-1010.

Keim, M., R.S. Williams, and A.J. Harwood. 2004. An inverse PCR technique to rapidly isolate the flanking DNA of dictyostelium insertion mutants. *Molecular biotechnology*. 26:221-224.

Kim, S.M., T.T. Nguyen, A. Ravi, P. Kubiniok, B.T. Finicle, V. Jayashankar, L. Malacrida, J. Hou, J. Robertson, D. Gao, J. Chernoff, M.A. Digman, E.O. Potma, B.J. Tromberg, P. Thibault, and A.L. Edinger. 2018. PTEN Deficiency and AMPK Activation Promote Nutrient Scavenging and Anabolism in Prostate Cancer Cells. *Cancer discovery*. 8:866-883.

King, B., J. Araki, W. Palm, and C.B. Thompson. 2020. Yap/Taz promote the scavenging of extracellular nutrients through macropinocytosis. *Genes & development*. 34:1345-1358.

King, J.S., and R.R. Kay. 2019. The origins and evolution of macropinocytosis. *Philosophical transactions of the Royal Society of London. Series B, Biological sciences*. 374:20180158.

King, J.S., D.M. Veltman, and R.H. Insall. 2011. The induction of autophagy by mechanical stress. *Autophagy*. 7:1490-1499.

Kuspa, A. 2006. Restriction enzyme-mediated integration (REMI) mutagenesis. *Methods in molecular biology*. 346:201-209.

Lee, S.W., Y. Zhang, M. Jung, N. Cruz, B. Alas, and C. Commisso. 2019. EGFR-Pak Signaling Selectively Regulates Glutamine Deprivation-Induced Macropinocytosis. *Developmental cell*. 50:381-392 e385.

Li, W., W. Zou, D. Zhao, J. Yan, Z. Zhu, J. Lu, and X. Wang. 2009. C. elegans Rab GTPase activating protein TBC-2 promotes cell corpse degradation by regulating the small GTPase RAB-5. *Development*. 136:2445-2455.

Lin, X.P., J.D. Mintern, and P.A. Gleeson. 2020. Macropinocytosis in Different Cell Types: Similarities and Differences. *Membranes*. 10.

Lord, S.J., K.B. Velle, R.D. Mullins, and L.K. Fritz-Laylin. 2020. SuperPlots: Communicating reproducibility and variability in cell biology. *J Cell Biol*. 219.

Maekawa, M., S. Terasaka, Y. Mochizuki, K. Kawai, Y. Ikeda, N. Araki, E.Y. Skolnik, T. Taguchi, and H. Arai. 2014. Sequential breakdown of 3-phosphorylated phosphoinositides is essential for the completion of macropinocytosis. *Proc Natl Acad Sci U S A*. 111:E978-987.

Mylvaganam, S., S.A. Freeman, and S. Grinstein. 2021. The cytoskeleton in phagocytosis and macropinocytosis. *Curr Biol*. 31:R619-R632.

Norbury, C.C., L.J. Hewlett, A.R. Prescott, N. Shastri, and C. Watts. 1995. Class I MHC presentation of exogenous soluble antigen via macropinocytosis in bone marrow macrophages. *Immunity*. 3:783-791.

Palm, W. 2019. Metabolic functions of macropinocytosis. *Philos T R Soc B*. 374.
Palm, W., J. Araki, B. King, R.G. DeMatteo, and C.B. Thompson. 2017. Critical role for PI3-kinase in regulating the use of proteins as an amino acid source. *Proc Natl Acad Sci U S A*. 114:E8628-E8636.
Palm, W., Y. Park, K. Wright, N.N. Pavlova, D.A. Tuveson, and C.B. Thompson. 2015. The Utilization of Extracellular Proteins as Nutrients Is Suppressed by mTORC1. *Cell*. 162:259-270.
Paschke, P., D.A. Knecht, A. Silale, D. Traynor, T.D. Williams, P.A. Thomason, R.H. Insall, J.R. Chubb, R.R. Kay, and D.M. Veltman. 2018. Rapid and efficient genetic engineering of both wild type and axenic strains of Dictyostelium discoideum. *PloS one*. 13:e0196809.
Ramirez, C., A.D. Hauser, E.A. Vucic, and D. Bar-Sagi. 2019. Plasma membrane V-ATPase controls oncogenic RAS-induced macropinocytosis. *Nature*. 576:477-481.
Rivero, F., and M. Maniak. 2006. Quantitative and microscopic methods for studying the endocytic pathway. *Methods in molecular biology*. 346:423-438.
Rosel, D., T. Khurana, A. Majithia, X. Huang, R. Bhandari, and A.R. Kimmel. 2012. TOR complex 2 (TORC2) in Dictyostelium suppresses phagocytic nutrient capture independently of TORC1-mediated nutrient sensing. *J Cell Sci*. 125:37-48.
Rupper, A., K. Lee, D. Knecht, and J. Cardelli. 2001. Sequential activities of phosphoinositide 3-kinase, PKB/Aakt, and Rab7 during macropinosome formation in Dictyostelium. *Mol Biol Cell*. 12:2813-2824.
Sallusto, F., M. Cella, C. Danieli, and A. Lanzavecchia. 1995. Dendritic cells use macropinocytosis and the mannose receptor to concentrate macromolecules in the major histocompatibility complex class II compartment: downregulation by cytokines and bacterial products. *The Journal of experimental medicine*. 182:389-400.
Sattler, N., C. Bosmani, C. Barisch, A. Gueho, N. Gopaldass, M. Dias, F. Leuba, F. Bruckert, P. Cosson, and T. Soldati. 2018. Functions of the Dictyostelium LIMP-2 and CD36 homologues in bacteria uptake, phagolysosome biogenesis and host cell defence. *J Cell Sci*. 131.
Shao, X., G. Cao, D. Chen, J. Liu, B. Yu, M. Liu, Y.X. Li, B. Cao, Y. Sadovsky, and Y.L. Wang. 2021. Placental trophoblast syncytialization potentiates macropinocytosis via mTOR signaling to adapt to reduced amino acid supply. *Proc Natl Acad Sci U S A*. 118.
Shaulsky, G., R. Escalante, and W.F. Loomis. 1996. Developmental signal transduction pathways uncovered by genetic suppressors. *Proc Natl Acad Sci U S A*. 93:15260-15265.
Smith, D.E., B. Clemencon, and M.A. Hediger. 2013. Proton-coupled oligopeptide transporter family SLC15: physiological, pharmacological and pathological implications. *Molecular aspects of medicine*. 34:323-336.
Steel, A., S. Nussberger, M.F. Romero, W.F. Boron, C.A. Boyd, and M.A. Hediger. 1997. Stoichiometry and pH dependence of the rabbit proton-dependent oligopeptide transporter PepT1. *The Journal of physiology*. 498 (Pt 3):563-569.

Swanson, J.A. 2014. Phosphoinositides and engulfment. *Cellular microbiology*. 16:1473-1483.
Terada, T., M. Irie, M. Okuda, and K. Inui. 2004. Genetic variant Arg57His in human H+/peptide cotransporter 2 causes a complete loss of transport function. *Biochemical and biophysical research communications*. 316:416-420.
Veltman, D.M., G. Akar, L. Bosgraaf, and P.J. Van Haastert. 2009. A new set of small, extrachromosomal expression vectors for Dictyostelium discoideum. *Plasmid*. 61:110-118.
Veltman, D.M., M.G. Lemieux, D.A. Knecht, and R.H. Insall. 2014. PIP(3)-dependent macropinocytosis is incompatible with chemotaxis. *J Cell Biol*. 204:497-505.
Veltman, D.M., T.D. Williams, G. Bloomfield, B.C. Chen, E. Betzig, R.H. Insall, and R.R. Kay. 2016. A plasma membrane template for macropinocytic cups. *Elife*. 5.
Verdon, Q., M. Boonen, C. Ribes, M. Jadot, B. Gasnier, and C. Sagne. 2017. SNAT7 is the primary lysosomal glutamine exporter required for extracellular protein-dependent growth of cancer cells. *Proc Natl Acad Sci U S A*. 114:E3602-E3611.
Williams, T.D., and R.R. Kay. 2018. The physiological regulation of macropinocytosis during Dictyostelium growth and development. *J Cell Sci*. 131.
Wolfson, R.L., and D.M. Sabatini. 2017. The Dawn of the Age of Amino Acid Sensors for the mTORC1 Pathway. *Cell metabolism*. 26:301-309.
Wyant, G.A., M. Abu-Remaileh, R.L. Wolfson, W.W. Chen, E. Freinkman, L.V. Danai, M.G. Vander Heiden, and D.M. Sabatini. 2017. mTORC1 Activator SLC38A9 Is Required to Efflux Essential Amino Acids from Lysosomes and Use Protein as a Nutrient. *Cell*. 171:642-654 e612.
Xu, L., I.S. Haworth, A.A. Kulkarni, M.B. Bolger, and D.L. Davies. 2009. Mutagenesis and cysteine scanning of transmembrane domain 10 of the human dipeptide transporter. *Pharmaceutical research*. 26:2358-2366.
Yao, W., J.L. Rose, W. Wang, S. Seth, H. Jiang, A. Taguchi, J. Liu, L. Yan, A. Kapoor, P. Hou, Z. Chen, Q. Wang, L. Nezi, Z. Xu, J. Yao, B. Hu, P.F. Pettazzoni, I.L. Ho, N. Feng, V. Ramamoorthy, S. Jiang, P. Deng, G.J. Ma, P. Den, Z. Tan, S.X. Zhang, H. Wang, Y.A. Wang, A.K. Deem, J.B. Fleming, A. Carugo, T.P. Heffernan, A. Maitra, A. Viale, H. Ying, S. Hanash, R.A. DePinho, and G.F. Draetta. 2019. Syndecan 1 is a critical mediator of macropinocytosis in pancreatic cancer. *Nature*. 568:410-414.
Yoshida, S., A.D. Hoppe, N. Araki, and J.A. Swanson. 2009. Sequential signaling in plasma-membrane domains during macropinosome formation in macrophages. *J Cell Sci*. 122:3250-3261.

Figures

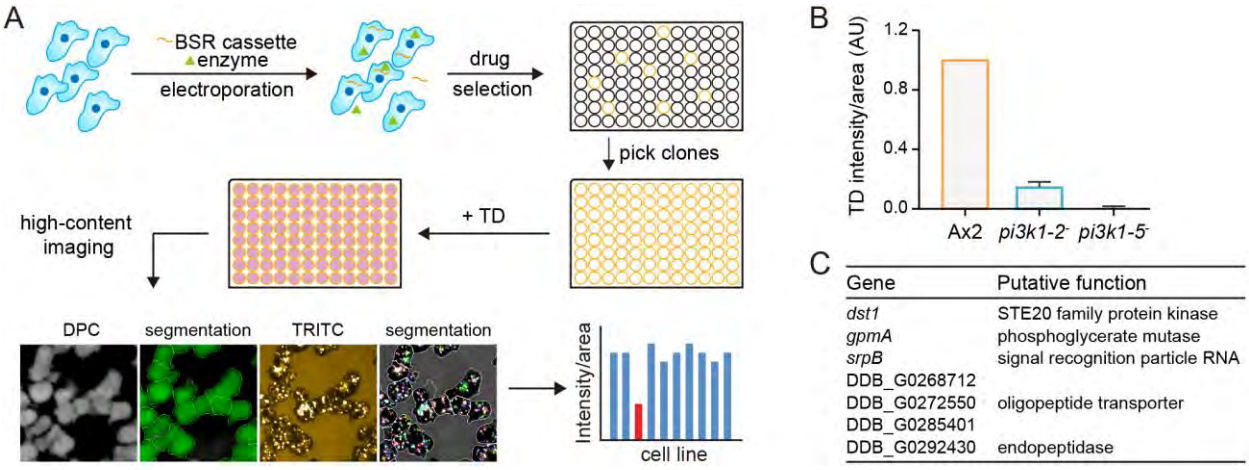

Gene	Putative function
dst1	STE20 family protein kinase
gpmA	phosphoglycerate mutase
srpB	signal recognition particle RNA
DDB_G0268712	
DDB_G0272550	oligopeptide transporter
DDB_G0285401	
DDB_G0292430	endopeptidase

Fig. 1. Screen for macropinocytosis regulators. (A) Schematic of the genetic screen. Mutant clones were generated by REMI, seeded in 96-well plates in growth medium, and incubated with TD. Images were captured in the digital phase contrast (DPC) and TRITC channels using a high-content screening system. The ratio of the total intensity of TD spots to the sum of cell area was used to quantitatively measure macropinocytosis. (B) Ax2, *pi3k1-2*-null, and *pi3k1-5*-null cells were analyzed for TD uptake using the screening system. Data was from three independent experiments. Mean ± SD. (C) List of mutants obtained from the screen.

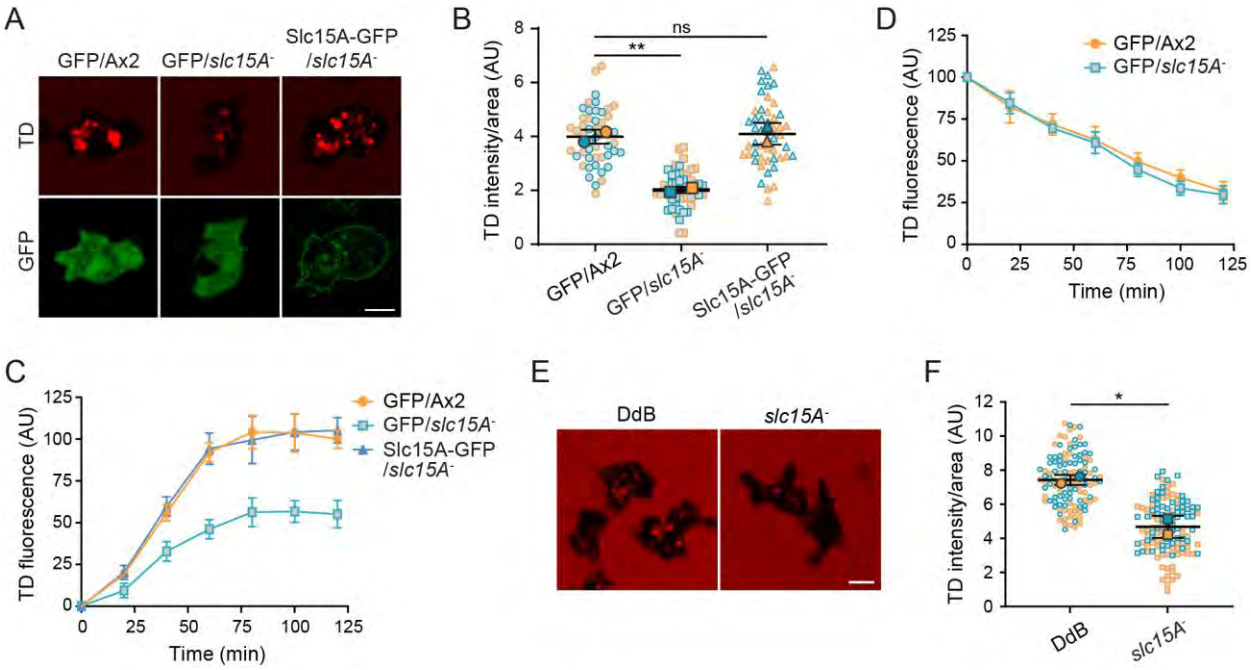

Fig. 2. Slc15A is involved in the regulation of macropinocytosis. (A-B) Confocal images and quantification of TD uptake in Ax2 and *slc15A*$^{-}$ cells expressing GFP or Slc15A-GFP. Data was from two independent experiments with at least 20 cells quantified per experiment (each experiment is color coded). Mean ± SD. (C-D) Quantification of TD macropinocytosis (C) and exocytosis (D) by fluorimetric analysis. Data was from four independent experiments. Mean ± SD. (E-F) Confocal images and quantification of TD uptake in DdB and *slc15A*$^{-}$ cells. Data was from two independent experiments with at least 50 cells quantified per experiment (each experiment is color coded). Mean ± SD. Statistical significance was determined by one-way ANOVA with Dunnett post-test in (B) and two-tailed unpaired t test in (F). Scale bar, 5 µm.

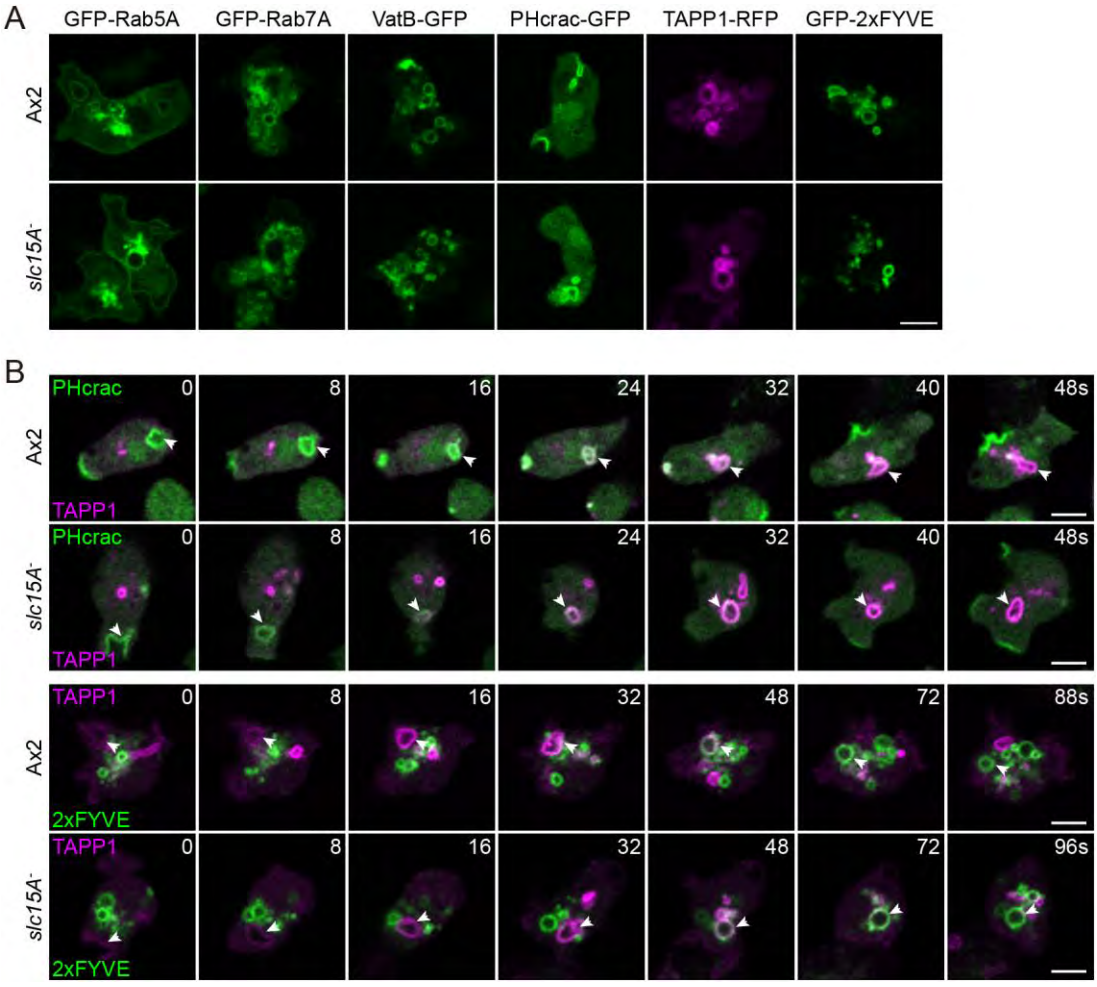

Fig. 3. Localization of macropinocytic marker proteins in Ax2 and *slc15A* deletion cells. (A) Confocal images of the indicated marker proteins in Ax2 and *slc15A*$^{-}$ cells. (B) Top: Time-lapse images showing the sequential accumulation of PHcrac-GFP and TAPP1-RFP in Ax2 and *slc15A*$^{-}$ cells. Bottom: Time-lapse images showing the sequential accumulation of TAPP1-RFP and GFP-2×FYVE in Ax2 and *slc15A*$^{-}$ cells. Scale bar, 5 µm.

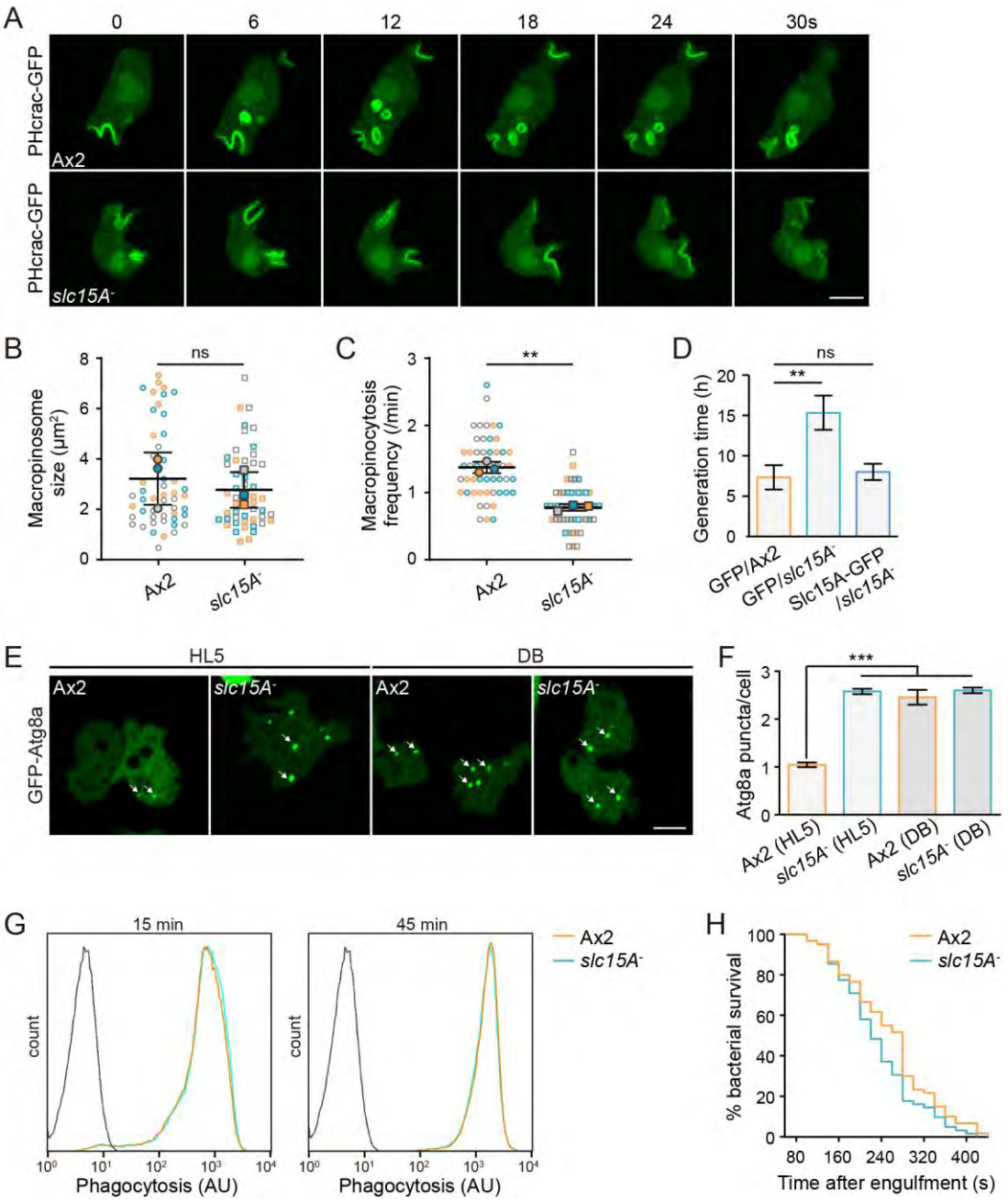

Fig. 4. Macropinocytosis is specifically impaired in *slc15A* deletion cells. (A) Time-lapse images of PHcrac-GFP in Ax2 and *slc15A*⁻ cells. (B-C) Quantification of the size of newly enclosed macropinosomes labeled by PHcrac-GFP and rate of macropinosome formation. Data was from three independent experiments with at least 15 cells quantified per experiment (each experiment is color coded). Mean ± SD. (D) Cell growth in HL5 medium measured by

generation time. Data was from three independent experiments. Mean ± SD. (E) Confocal images of GFP-Atg8a in cells cultured in HL5 or non-nutrient development buffer (DB) for 1 h. (F) Quantification of average Atg8a puncta per cell. Data was from three independent experiments with at least 30 cells quantified per experiment. Mean ± SD. (G) Quantification of bacterial phagocytosis. Cells were incubated with mCherry-expressing *E.coli* for the indicated time points and phagocytosis was measured by flow cytometry. The black peak shows the background fluorescence. (H) Quantification of bacterial survival. Cells were incubated with GFP-expressing *E.coli*. The Kaplan-Meyer graph was based on the persistence of bacterial GFP-fluorescence within cells after phagocytosis. 60 bacteria were followed in each cell line. Statistical significance was determined by two-tailed unpaired t test in (B) and (C) and one-way ANOVA with Dunnett post-test in (D) and (F). Scale bar, 5 μm.

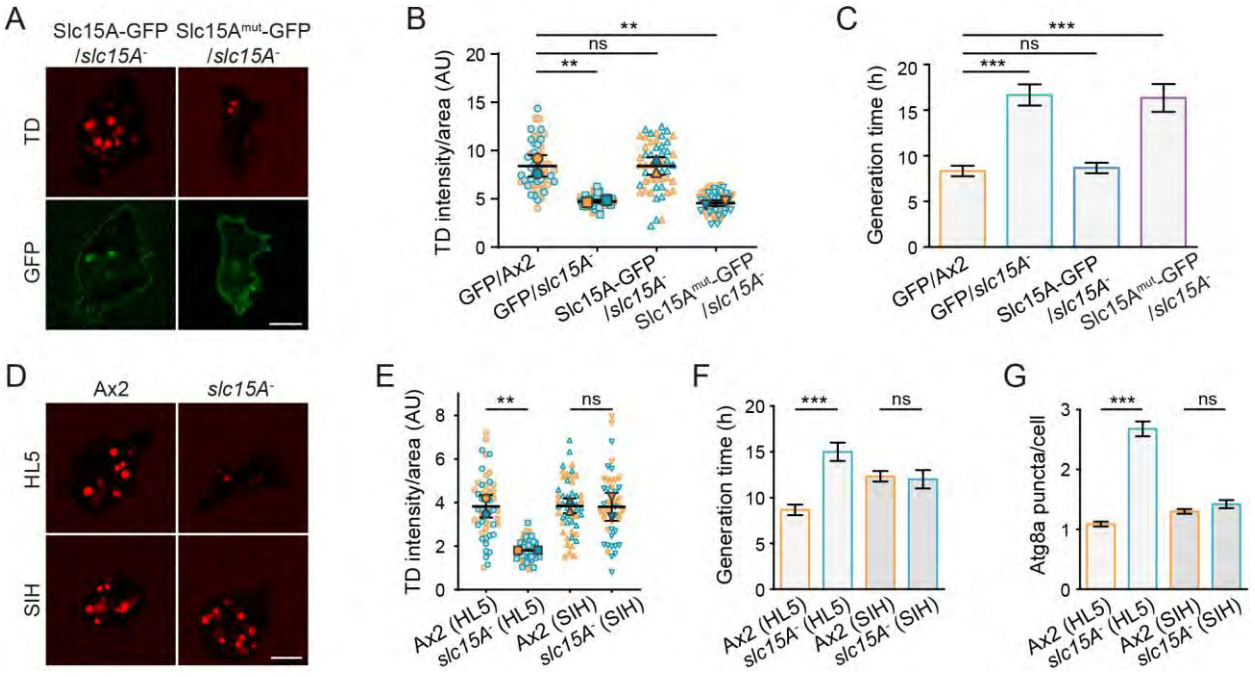

Fig. 5. The oligopeptide transport activity is required for Slc15A to modulate macropinocytosis. (A) Confocal images of TD uptake in *slc15A*$^{-}$ cells expressing Slc15A-GFP or Slc15A^{mut}-GFP bearing R68H and E438R mutations. (B) Quantification of TD uptake in cells transformed with the indicated plasmids. Data was from two independent experiments with at least 20 cells quantified per experiment (each experiment is color coded). Mean ± SD. (C) Cell growth in HL5 measured by generation time. Data was from three independent experiments. Mean ± SD. (D-E) Confocal images and quantification of TD uptake in Ax2 and *slc15A*$^{-}$ cells grown in HL5 or SIH medium. Data was from two independent experiments with at least 20 cells quantified per experiment (each experiment is color coded). Mean ± SD. (F) Cell growth in HL5 or SIH measured by generation time. Data was from three independent experiments. Mean ± SD. (G) Quantification of average GFP-Atg8a puncta per cell in cells grown in HL5 or SIH. Data was from three independent experiments with at least 30 cells quantified per experiment. Statistical significance was determined by one-way ANOVA with Dunnett post-test in (B) and (C) and two-tailed unpaired t test in (E), (F), and (G). Scale bar, 5 μm.

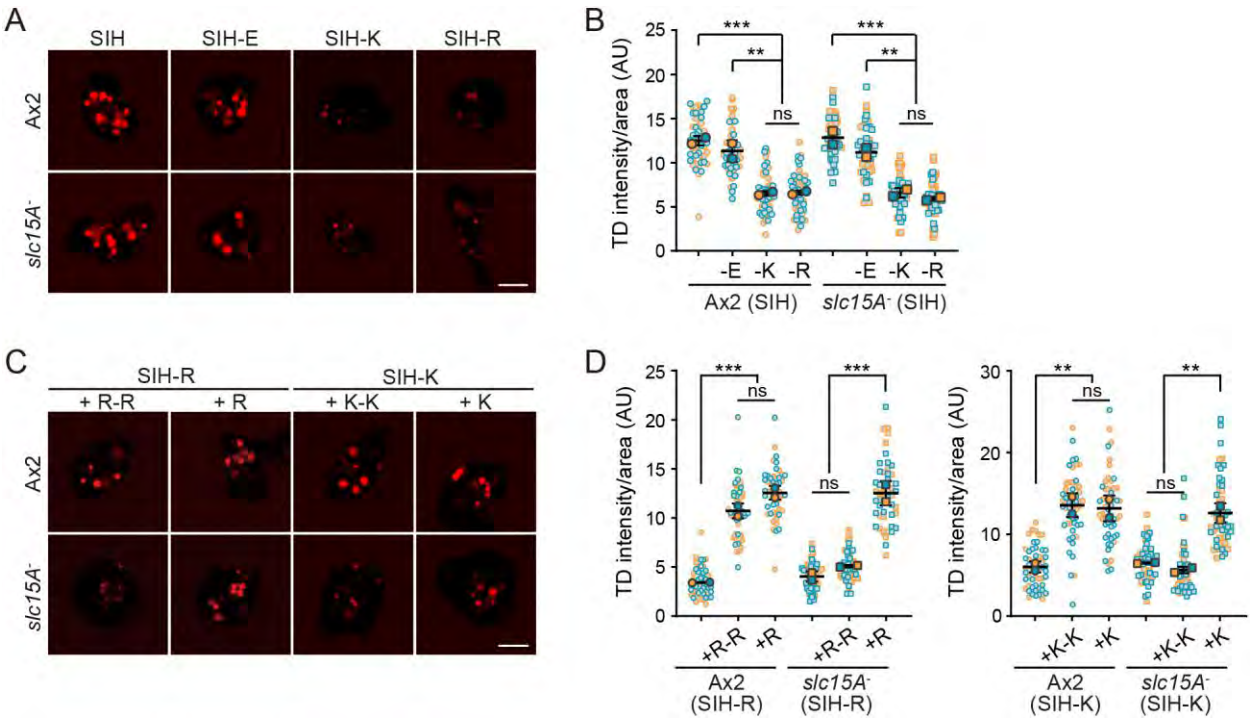

Fig. 6. Slc15A functions to maintain nutrient availability and promote macropinocytosis. (A-B) Confocal images and quantification of TD uptake in Ax2 and *slc15A*$^{-}$ cells cultured in SIH or SIH omitting the indicated amino acid. (C-D) Confocal images and quantification of TD uptake in Ax2 and *slc15A*$^{-}$ cells cultured in SIH-R or SIH-K medium supplemented with the indicated amino acid or dipeptide. For plots in (B) and (D), data was from two independent experiments with at least 20 cells quantified per experiment (each experiment is color coded). Mean ± SD. Statistical significance was determined by one-way ANOVA with Tukey post-test. Scale bar, 5 µm.

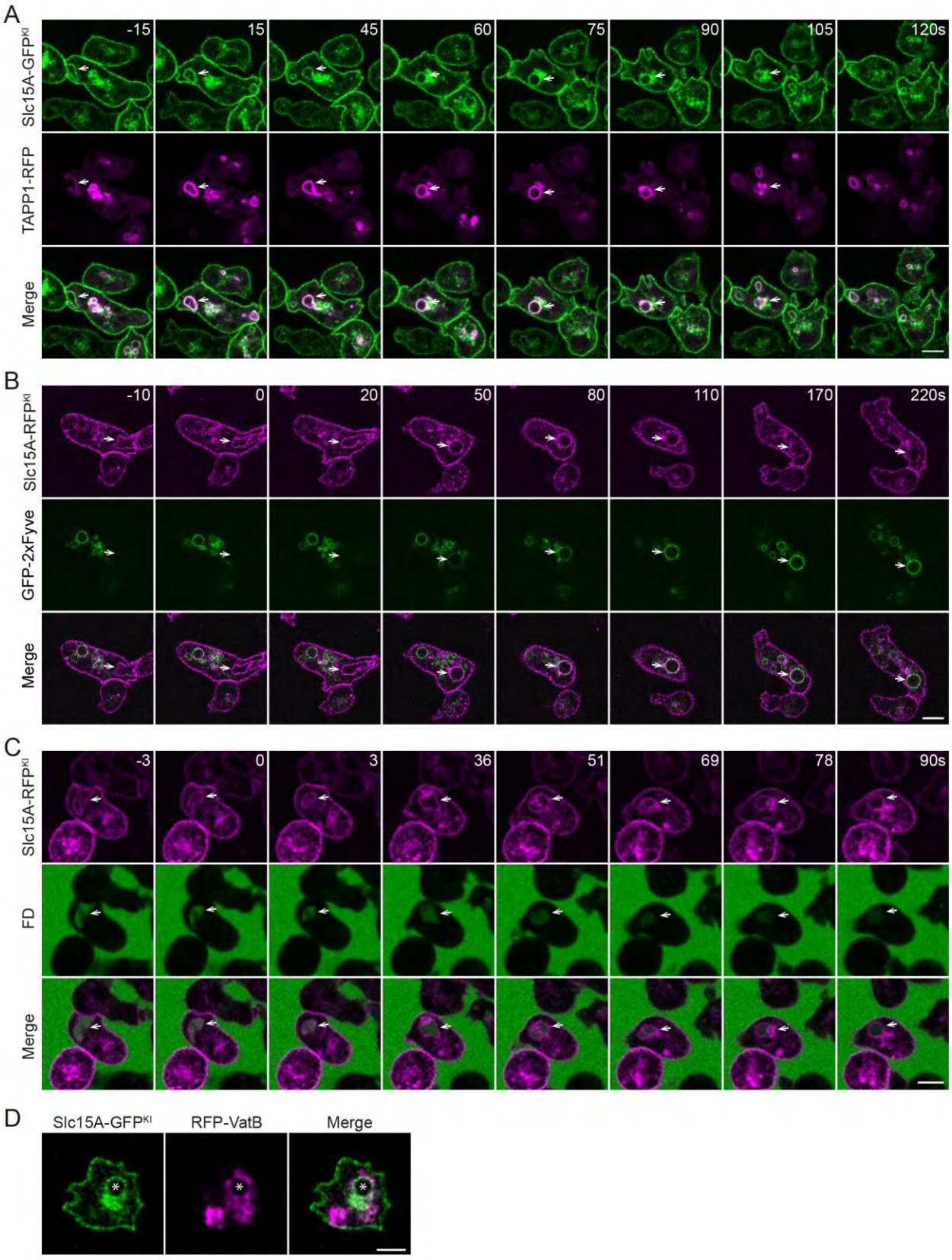

Fig. 7. Slc15A functions in the early macropinocytic pathway. (A) Time-lapse images of Slc15A-GFP^{KI} and TAPP1-RFP in Ax2 cells during macropinocytosis. The arrows point to a newly generated macropinosome, with which Slc15A and TAPP1 associated for approximately 100 sec. (B) Time-lapse images of Slc15A-RFP^{KI} and GFP-2×FYVE in Ax2 cells during macropinocytosis. The arrows point to a newly generated macropinosome, which was converted from Slc15A-positive to 2×FYVE-positive. (C) Time-lapse images of Slc15A-RFP^{KI} in cells incubated with FD. The arrows point to a newly generated macropinosome that quickly acquired an acidic environment indicated by the decrease of the fluorescence of FD. (D) Confocal images of Slc15A-GFP^{KI} and RFP-VatB. The asterisks indicate a nascent macropinosome marked by both Slc15A-GFP and RFP-VatB. Scale bar, 5 μm.

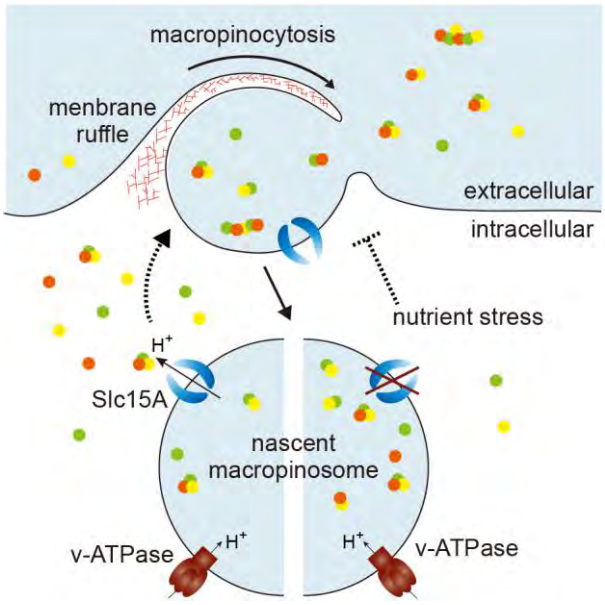

Fig. 8. Working model. Slc15A, a proton-coupled oligopeptide transporter localized at the plasma membrane and early macropinosome, mediates oligopeptide transport from the growth medium to the cytosol, thereby maintaining the intracellular availability of key amino acids and promoting macropinocytosis via a feedback regulation. Disruption of *slc15A* causes reduced oligopeptide transport and a nutrient stress condition, which in turn impairs macropinocytosis and leads to defects in cell growth and autophagy regulation. Amino acids and peptides are indicated by colored circles.

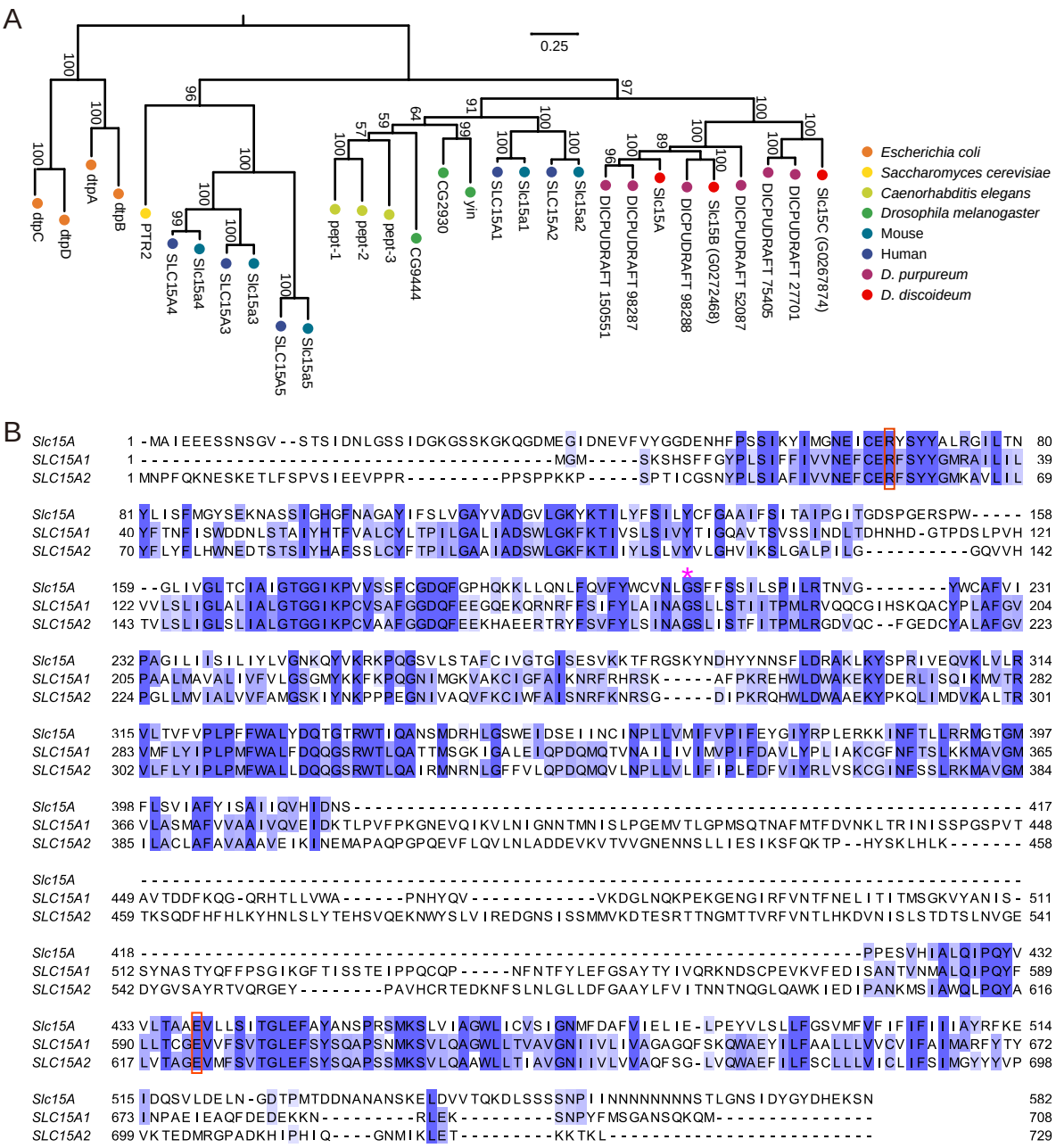

Fig. S1. Conservation of SLC15 family proteins. (A) Phylogenetic tree of the SLC15 family. Shown is a maximum likelihood tree built with LG+F+G4 model. Bootstrap values are from 1,000 iterations. In addition to Slc15A, *Dictyostelium* genome encodes two other proteins that are homologous to human SLC15 proteins. We named them Slc15B (DDB_G0272468) and Slc15C (DDB_G0267874). (B) Sequence alignment of Slc15A with human SLC15A1 and SLC15A2. Red boxes mark the two conserved residues, R68 and E438, in Slc15A. Mutation of the corresponding amino acid, R57H in SLC15A2 or E595R in SLC15A1, was shown to abolish the oligopeptide transport function of the protein. The red asterisk marks the position of REMI insertion.

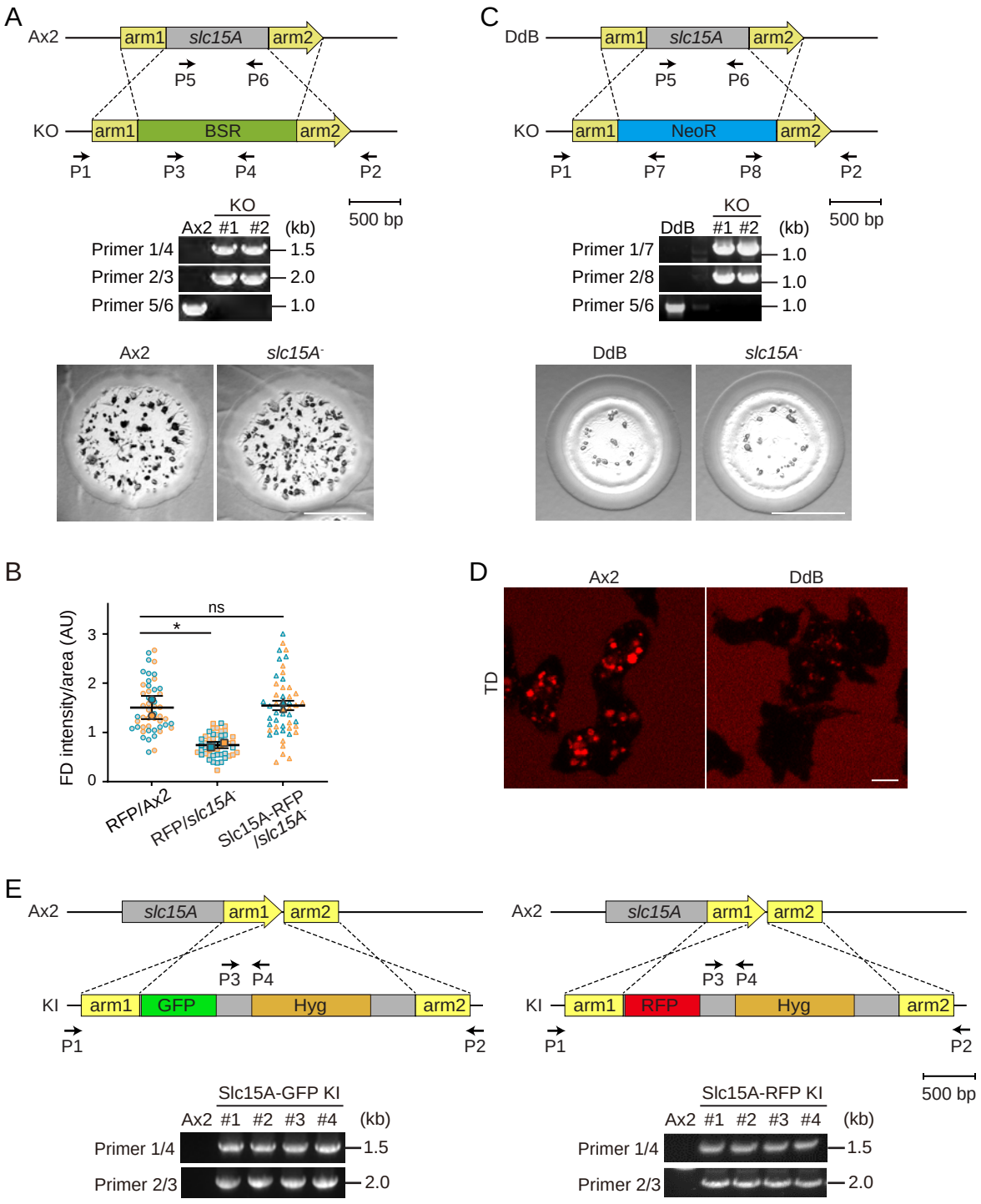

Fig. S2. Generation of slc15A deletion and knock-in cells. (A) Generation of *slc15A*$^{-}$ cell line in the Ax2 background. Top: A blasticidin resistant cassette (BSR) was used to replace part of the open reading frame of *slc15A*, and targeted clones were verified by PCR. Bottom: Ax2 and *slc15A*$^{-}$ cells were plated clonally with *K. aerogenes* on standard medium agar. Representative images were captured after 5 d. Scale bar, 5 mm. (B) Quantification of FD uptake in Ax2 and *slc15A*$^{-}$ cells expressing RFP or Slc15A-RFP. Data was from two independent experiments with at least 20 cells quantified per experiment (each experiment is color coded). Mean ± SD. Statistical significance was determined by one-way ANOVA with Dunnett post-test. (C) Generation of *slc15A*$^{-}$ cell line in the DdB background. Top: A neomycin resistant cassette (NeoR) was used to replace part of the open reading frame of *slc15A*, and targeted clones were verified by PCR. Bottom: DdB and *slc15A*$^{-}$ cells were plated clonally with *K. aerogenes* on standard medium agar. Representative images were captured after 4 d. Scar bar, 5 mm. (D) Confocal images of TD uptake in Ax2 and DdB cells. (E) Design of knock-in constructs. Slc15A-GFP^{KI} and Slc14A-RFP^{KI} cells were generated by targeted in-frame integration of GFP or RPF at the C-terminus of Slc15A. Targeted clones were verified by PCR. Scale bar, 5 µm.

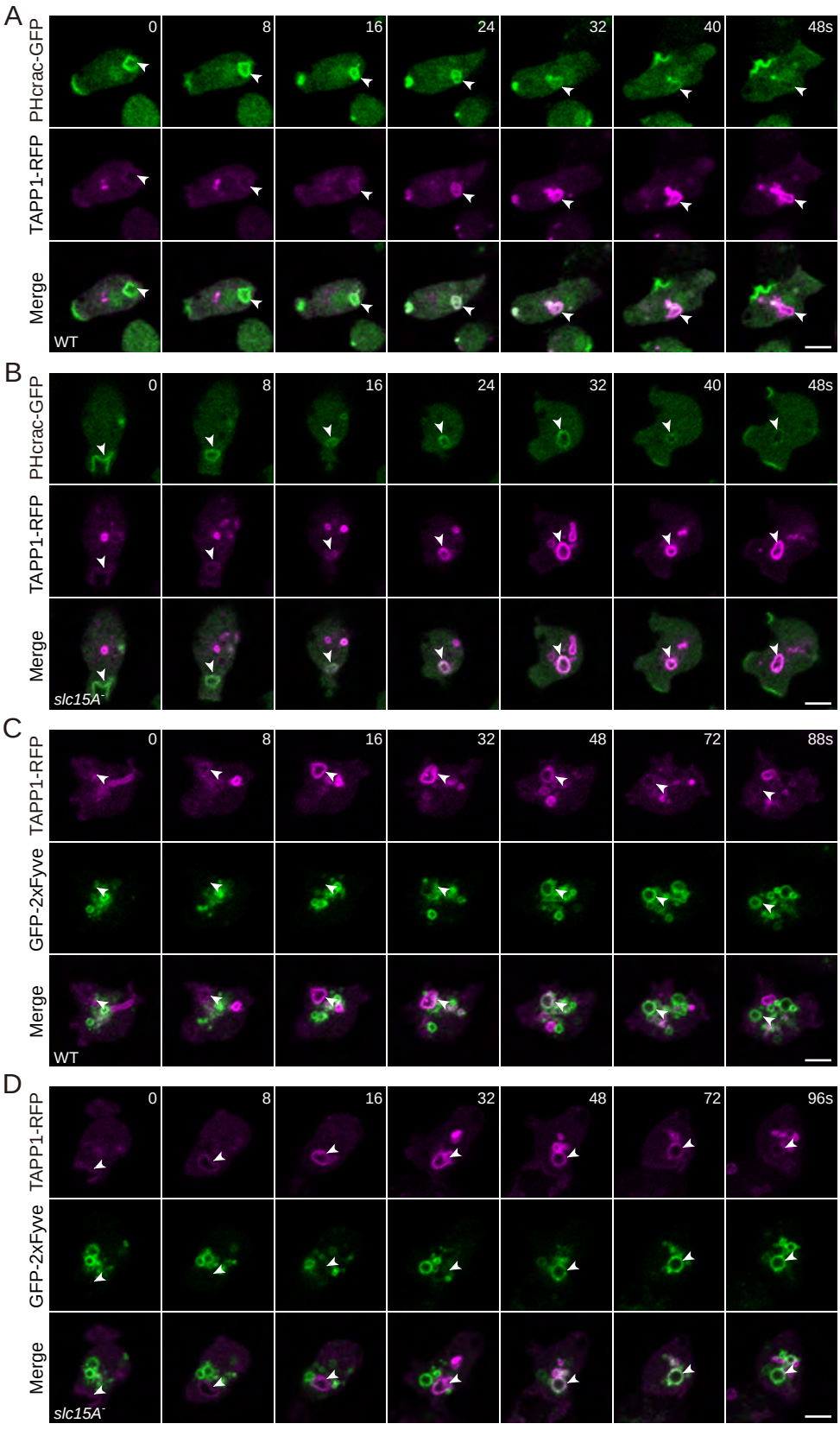

Fig. S3. PIP conversion during macropinocytosis in Ax2 and *slc15A*⁻ cells. (A-B) Time-lapse images showing the sequential accumulation of PHcrac-GFP and TAPP1-RFP in Ax2 and *slc15A*⁻ cells. (C-D) Time-lapse images showing the sequential accumulation of TAPP1-RFP and GFP-2xFYVE in Ax2 and *slc15A*⁻ cells. Scale bar, 5 µm.

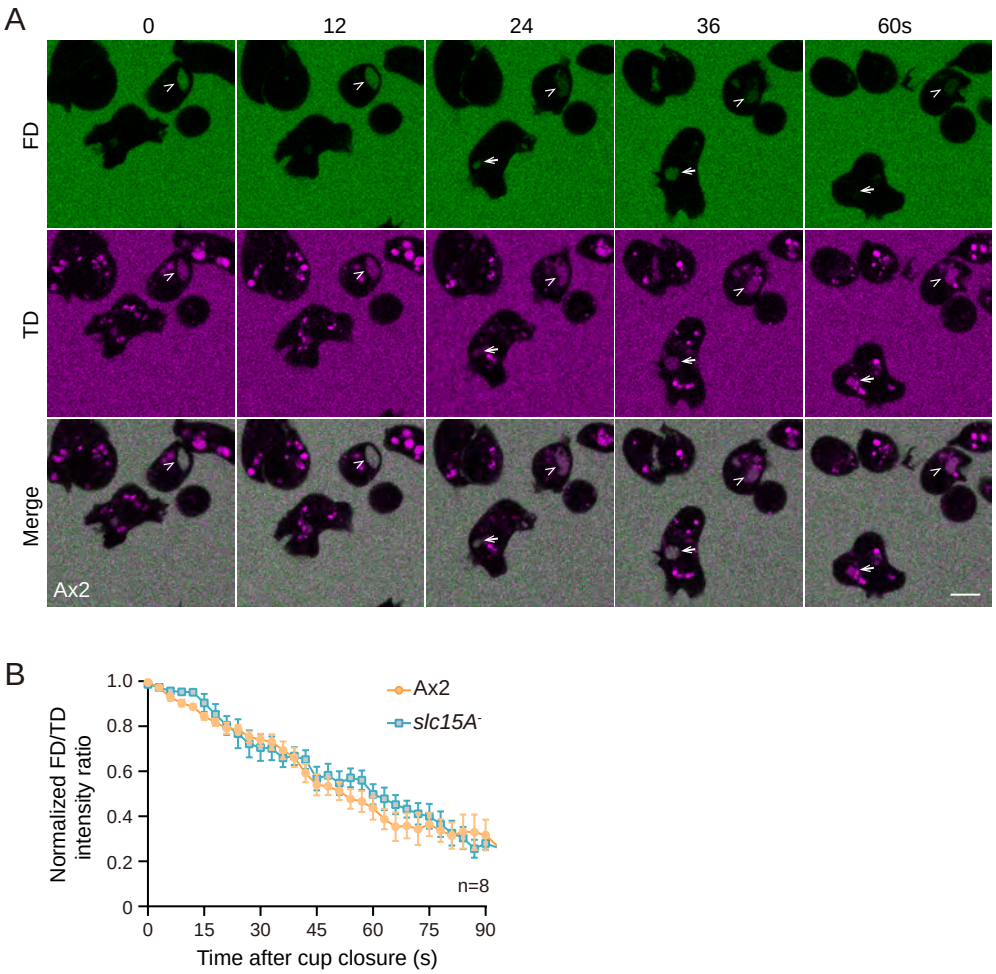

Fig. S4. Macropinosome acidification in Ax2 and *slc15A*$^{-}$ cells. (A) Time-lapse images of Ax2 cells incubated with 1 mg/ml FD and 0.5 mg/ml TD. Arrows mark newly formed macropinosomes that quickly acquired an acidic environment indicated by the decrease of the fluorescence of FD. (B) Macropinosome acidification quantified by measuring the ratio of FD/TD as a function of time after cup closure in Ax2 and *slc15A*$^{-}$ cells. Scale bar, 5 µm.

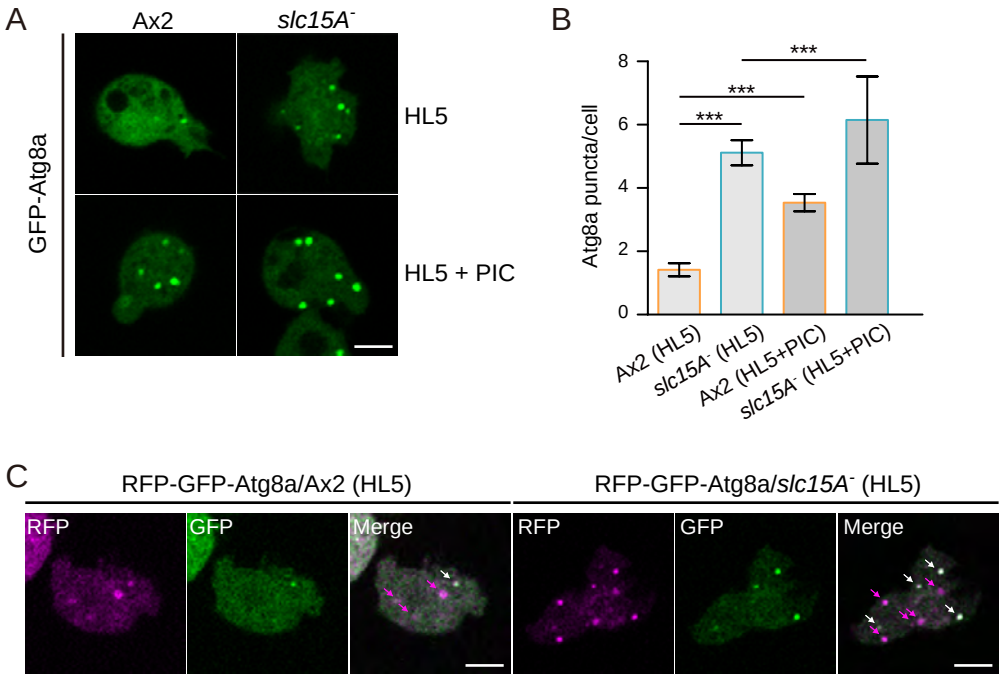

Fig. S5. Autophagy flux in Ax2 and *slc15A*⁻ cells. (A) Confocal images of GFP-Atg8a. Cells were cultured in HL5 in the absence or presence of a protease inhibitor cocktail (PIC). (B) Quantification of average Atg8a puncta per cell. At least 25 cells were quantified per condition. Mean ± SD. The addition of PIC further increased the number of GFP-Atg8a puncta in *slc15A*⁻ cells, indicating that autophagy flux was not blocked. (C) Confocal images of Atg8a fused to a tandem RFP-GFP tag. The presence of red-only puncta marked by the red arrows indicates that autophagy flux was not blocked in *slc15A*⁻ cells. White arrows point to Atg8a structures with both GFP and RFP signals. Scale bar, 5 µm.

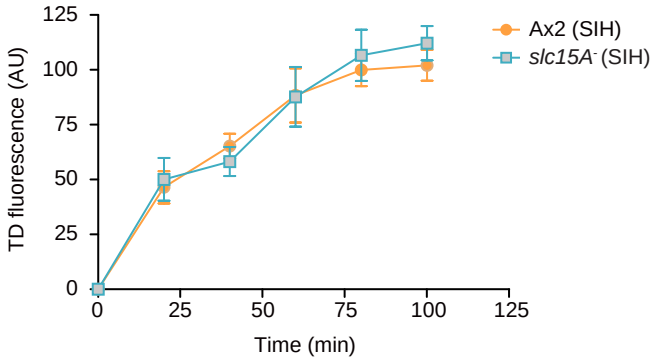

Fig. S6. Macropinocytosis in cells grown in SIH medium. Quantification of TD uptake in Ax2 and *slc15A*$^{-}$ cells by fluorimetric analysis. Data was from four independent experiments. Mean ± SD.

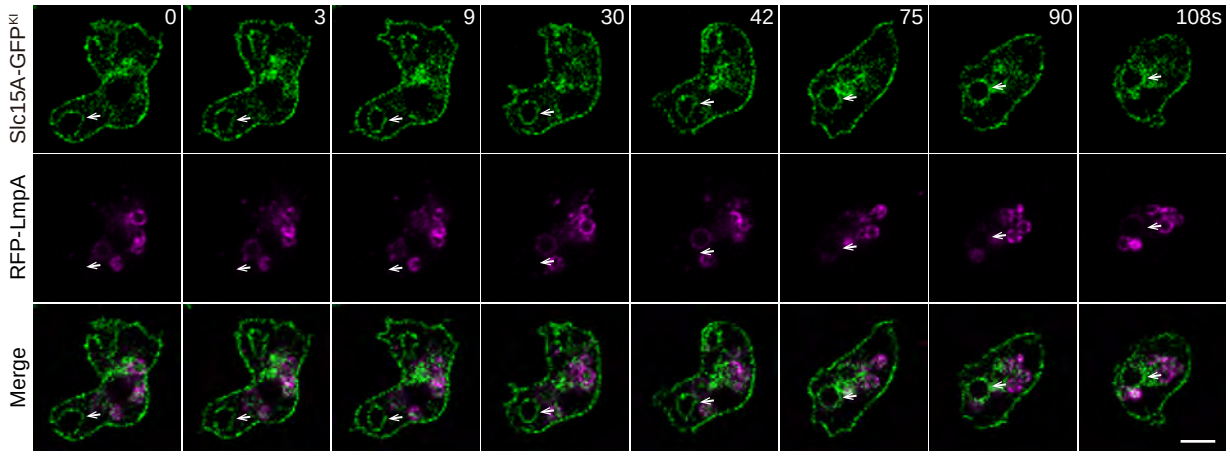

Fig. S7. Slc15A does not colocalize with the lysosomal/postlysosomal marker LmpA. Time-lapse images of Slc15A-GFP^{KI} and RFP-LmpA. The arrows point to a newly generated macropinosome marked by Slc15A. Scale bar, 5 µm.

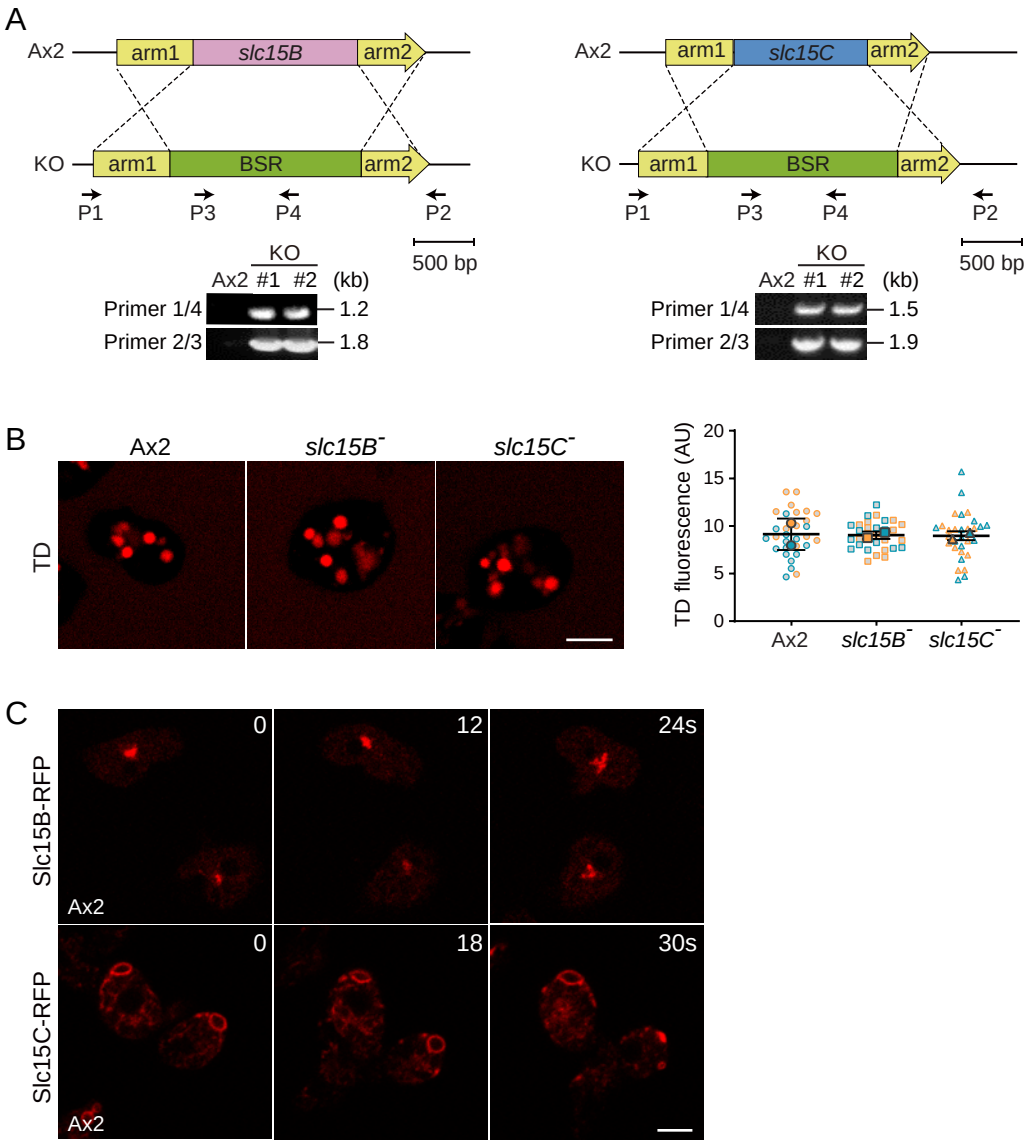

Fig. S8. Characterization of Slc15B and Slc15C. (A) Design of knockout constructs. The BSR was inserted via homologous recombination to replace part of the open reading frame of *slc15B* or *slc15C*. Targeted clones were verified by PCR. (B) Confocal images and quantification of TD uptake in Ax2, *slc15B*$^{-}$, and *slc15C*$^{-}$ cells. Data was from two independent experiments with at least 15 cells quantified per experiment (each experiment is color coded). Mean ± SD. (C) Time-lapse images of Slc15B-RFP and Slc15C-RFP expressed in Ax2 cells. Slc15B localizes to the Golgi and Slc15C localizes to the contractile vacuole structure. Scale bar, 5 µm.

Table S1. Plasmids and primers used in this study. Each primer is designated as forward (F) or reverse (R).

Usage	Plasmid backbone	Sequence, 5' - 3'
Expression in *Dictyostelium* cells		
Slc15A-GFP	pDM323	F: GCTCTAGAATGGCGATAGAAGAAGAATCATCAAATTCT R: ATAAGAATGCGGCCGCATTTGATTTTTCATGATCATAACCATAATCA
Slc15B-RFP	pDM324	F: GCTCTAGAATGGGTGGAATCGACGAAGATGG R: ATAAGAATGCGGCCGCTTTTGCATTTGATTTATTTGAATTTATTG
Slc15C-RFP	pDM324	F: GCTCTAGAATGAAAACAGACGATAAATATGCAAG R: ATAAGAATGCGGCCGCAATTAAATTATTTTCCAACTCTATAGATC
Slc15A$^{R68H/E438R}$-GFP	pDM323	R68H F: AATTTGTGAACATTATTCATACTATGCTTT R68H R: TGAATATAGTTCACAAATTTCATTACCCAT E438R F: GTCTTGACTGCCGCTCGTGTTTTATTATCA E438R R: ACACGAGCGGCAGTCAAGACAACATATTGTG
GFP-Rab5A	pDM317	F: CGGGAGCTCATGAATAATAATAATAAGATATTTC R: CGGACTAGTGTTACAACATTTGTTTTTCTTTCC
GFP-Rab7A	pDM317	F: CGGGAGCTCATGGCCACAAAGAAAAAGG R: CGGACTAGTACAACAACCTGATTTAGCTGG
TAPP1-RFP	pDM324	F: CGGGAGCTCATGCCTTATGTGGATCGTCAGAATC R: CTAGCTAGCCACGTCACTGACCGGAAGGCTCGC
GFP-Atg8a	pDM317	F: CTAAGATCTAGTGCTGGTGGTATGGTTCATGTATCAAGCTTTAAA R: CTAACTAGTTAAATCACTACCAAAAGATTTTCACC
RFP-GFP-Atg8a	pDM449	F: CGGGAGCTCATGGTTCATGTATCAAGCTTTAAAAAC R: CGGACTAGTTTATAAATCACTACCAAAAGTATTTTC GFP F: TGCTCTAGAATGGGTAAAGGAGAAGAACTTTTCAC GFP R: GGAAGATCTGGATCTGAGTCCGGACTTGTATAG
VatB-GFP	pDM323	F: CGGGAGCTCATGGTTGGATTTGAAGATCATATCG R: CGGACTAGTGTTAGTTGAATCTACAGTACCCTTTG
RFP-LmpA	pDM318	F: CGGGAGCTCATGGTAAAAAGAGGGTGTTGCCATAGAAAAATG R:CGGACTAGTTGGTTCTGTTAAACGACGACGTAATTCTTCTTCTAAACGACTTGG TTCATTATTAATAATTGCTTGATAAC
Generation of knockout cell		
slc15A knockout in Ax2	pBluescript-BSR	Insert 1 F: ACGGTCGACATGGCGATAGAAGAAGAATCATC Insert 1 R: ACGGAATTCAACACCATCAGCAACATAAGCAC Insert 2 F: ACGGGATCCGTGATTGCATTTTACATTTCAGC Insert 2 R: ACGACTAGTCAATACTATTACCCAAAGTTGAG
slc15A knockout in DdB	pDM1082	Insert 1 F: GGGGCCGGCATGGCGATAGAAGAAGAATC Insert 1 R: CCCAAGCTTAACACCATCAGCAACATAAGCA Insert 2 F: GGAAGATCTTGATTGCATTTTACATTTC Insert 2 R: CGGACTAGTTCAATACTATTACCCAAAGTTGAG
slc15B knockout	pBluescript-BSR	Insert 1 F: ACGCGTCGACATGGGTGGAATCGACGAAGATGGT Insert 1 R: CGGAATTCCTGCAATATATGCTCCAAATAATGTA Insert 2 F: GGACTAGTGAAGTTGATCAACAAAGATTAGATAATG Insert 2 R: ATAAGAATGCGGCCGCGCATTTGATTTATTTGAATTTATTGTGTAT
slc15C knockout	pBluescript-BSR	Insert 1 F: ACGCGTCGAC ATGAAAACAGACGATAAATATGCAAG Insert 1 R: CGGAATTCCAACAACTCCATCAATTGATGTTACTGAT Insert 2 F: GGACTAGTCACAATATTTAATTATAACGATTGCA Insert 2 R: ATAAGAATGCGGCCGCAATTAAATTATTTTCCAACTCTATAGATC
Generation of knock-in cell		
slc15A GFP and RFP knock-in	pDM1355	Insert 1 F: GGACTAGTCGTACCAATCTTTGAATATGGT Insert 1 R: GGACTAGTATTTGATTTTTCATGATCATAACC Insert 2 F: GGAGCCGGCTCAATTTAAAAATAAAAACACTTTGTA Insert 2 R: GGAGCCGGCATGCAAATTCTCCATTACCTCA
Expression in *E.coli*		
mCherry	pET-15b	F: CGCCATATGATGGTGAGCAAGGGCGAGGAG R: CCGCTCGAGGGGCCCCTTGTACAGCTCGTCC
GST-GFP	pGEX 4T-1	F: CCGGAATTCATGGTGAGCAAGGGCGAGGAG R: CCGCTCGAGCTTGTACAGCTCGTCCATGC

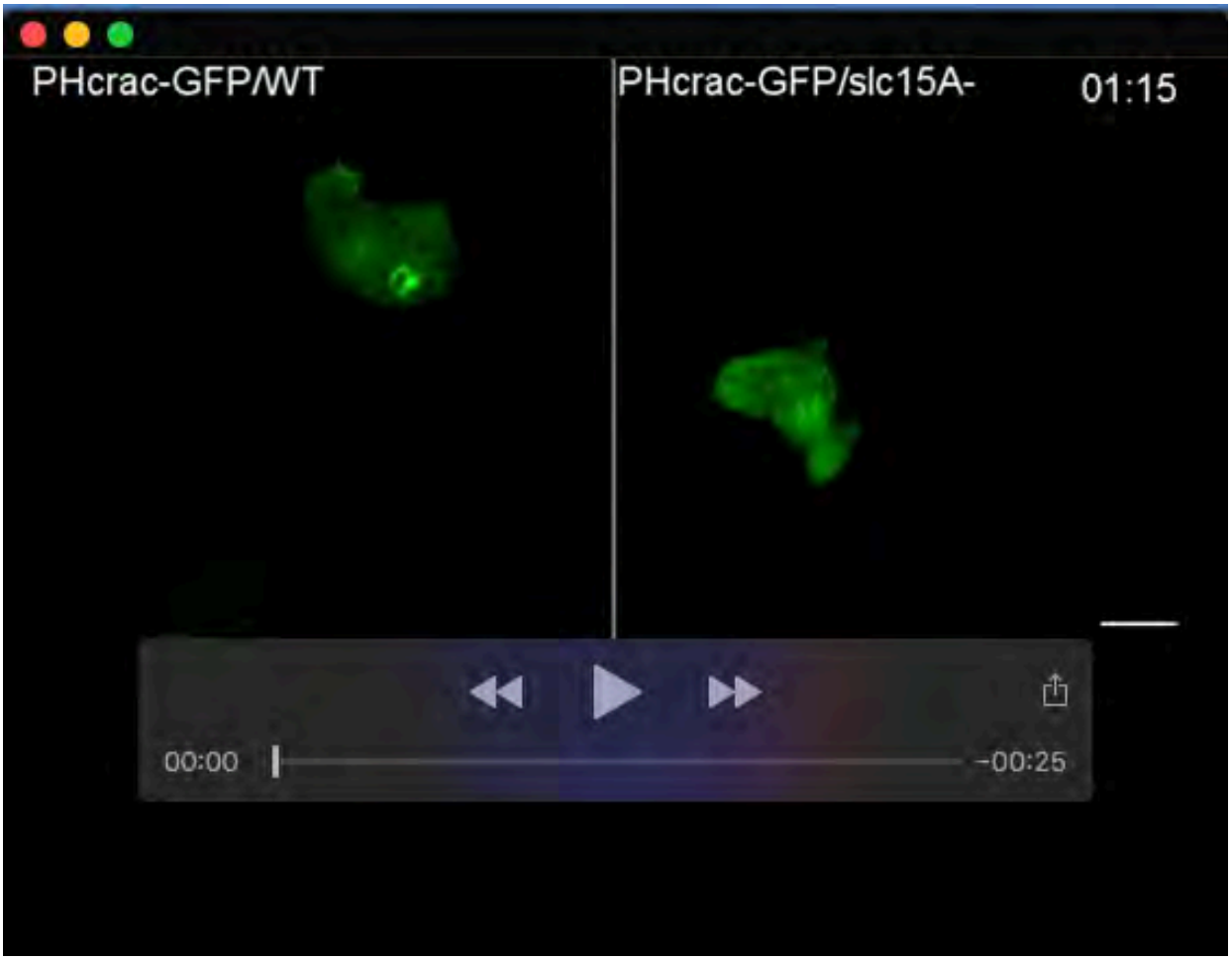

Movie 1. Time-lapse imaging of PHcrac-GFP dynamics in Ax2 and *slc15A*$^{-}$ cells. Corresponds to figure 4A. Images were captured at 3 sec per frame and played back at 15 frames per second. Scale bar, 5 µm.

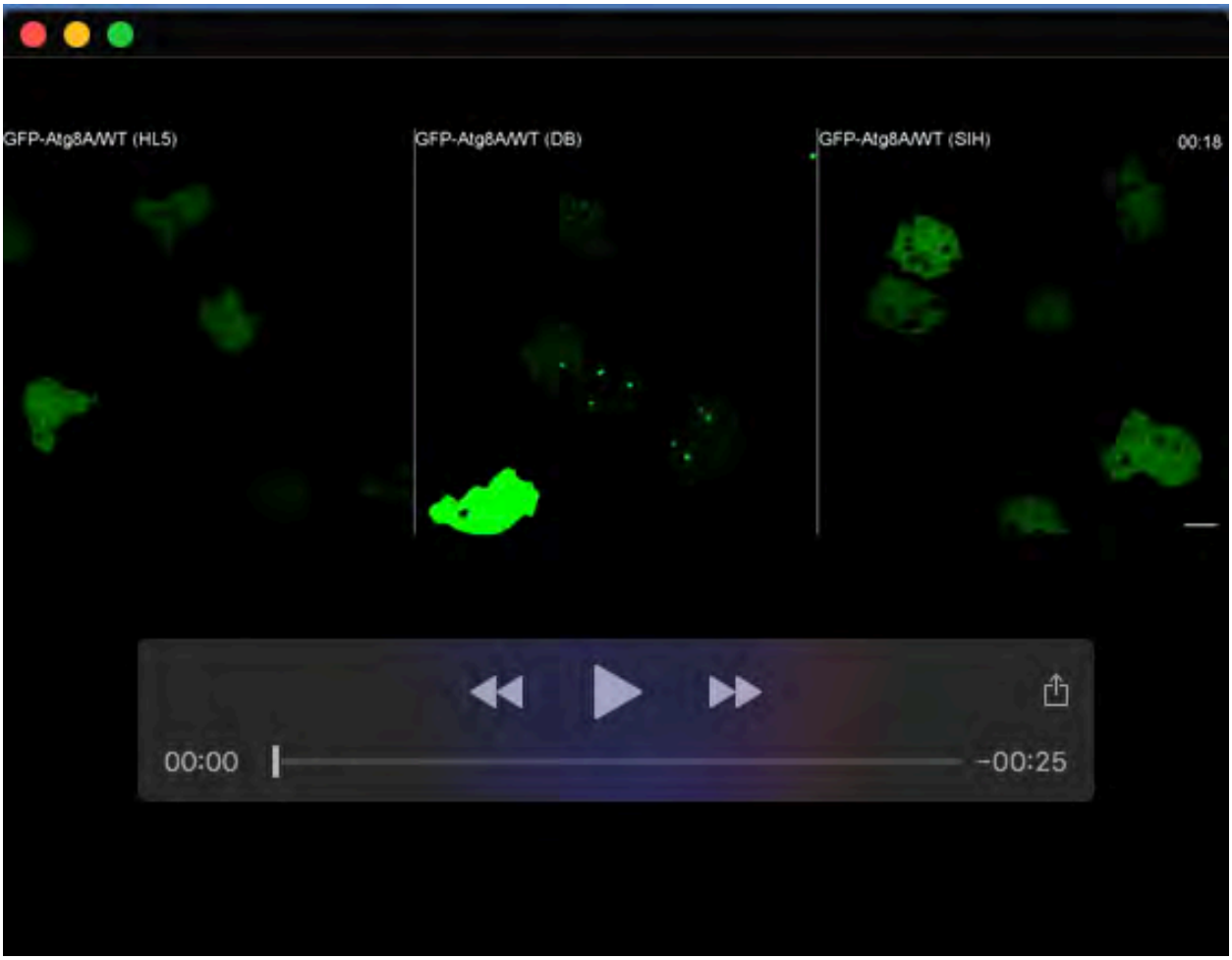

Movie 2. Time-lapse imaging of GFP-Atg8a in Ax2 cells cultured in HL5 medium, SIH medium, or non-nutrient development buffer (DB). Corresponds to figures 4E-F and 5G. Images were captured at 6 sec per frame and played back at 1 frame per second. Scale bar, 5 μm.

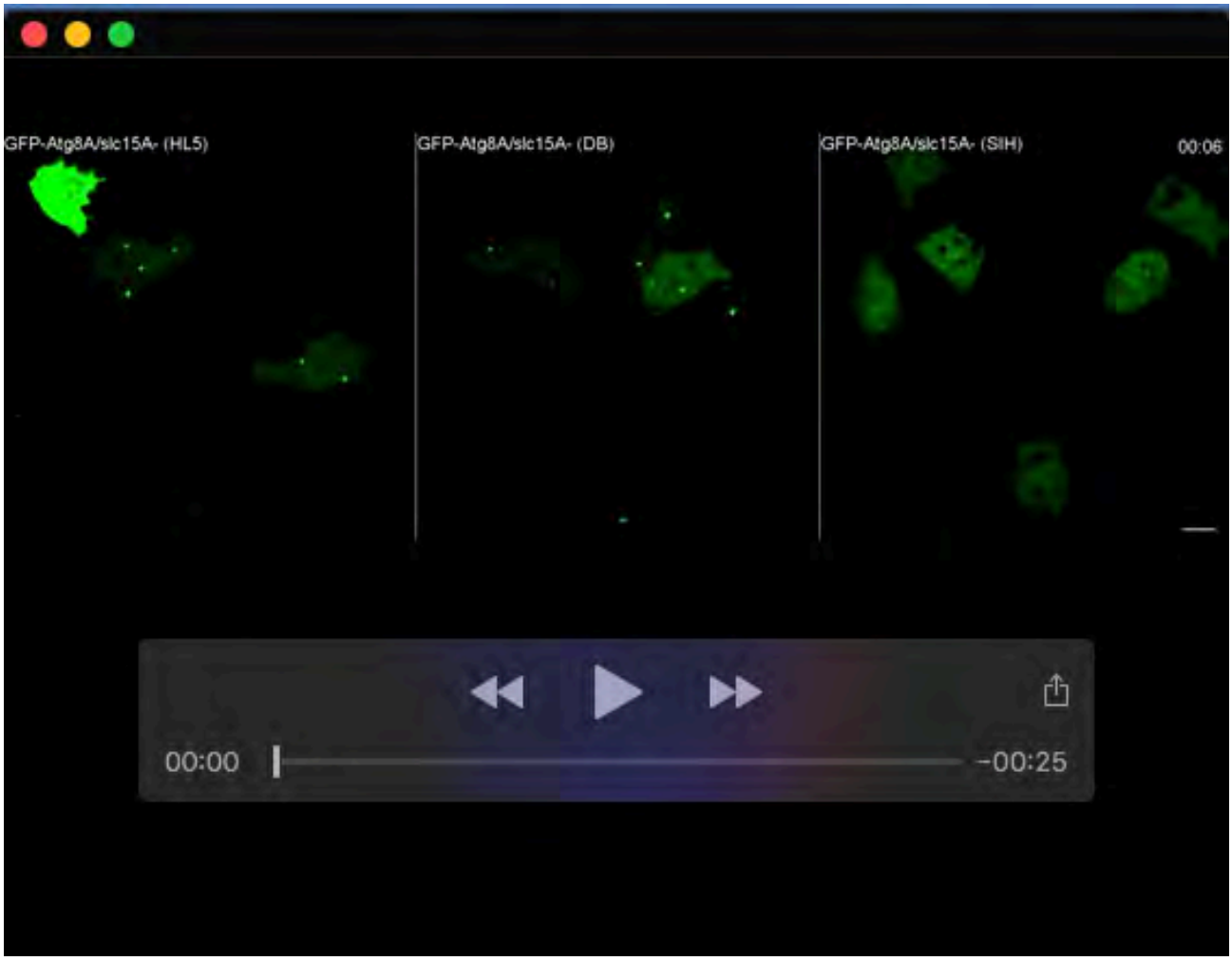

Movie 3. Time-lapse imaging of GFP-Atg8a in *slc15A*$^{-}$ cells cultured in HL5 medium, SIH medium, or non-nutrient development buffer (DB). Corresponds to figures 4E-F and 5G. Images were captured at 6 sec per frame and played back at 1 frame per second. Scale bar, 5 µm.

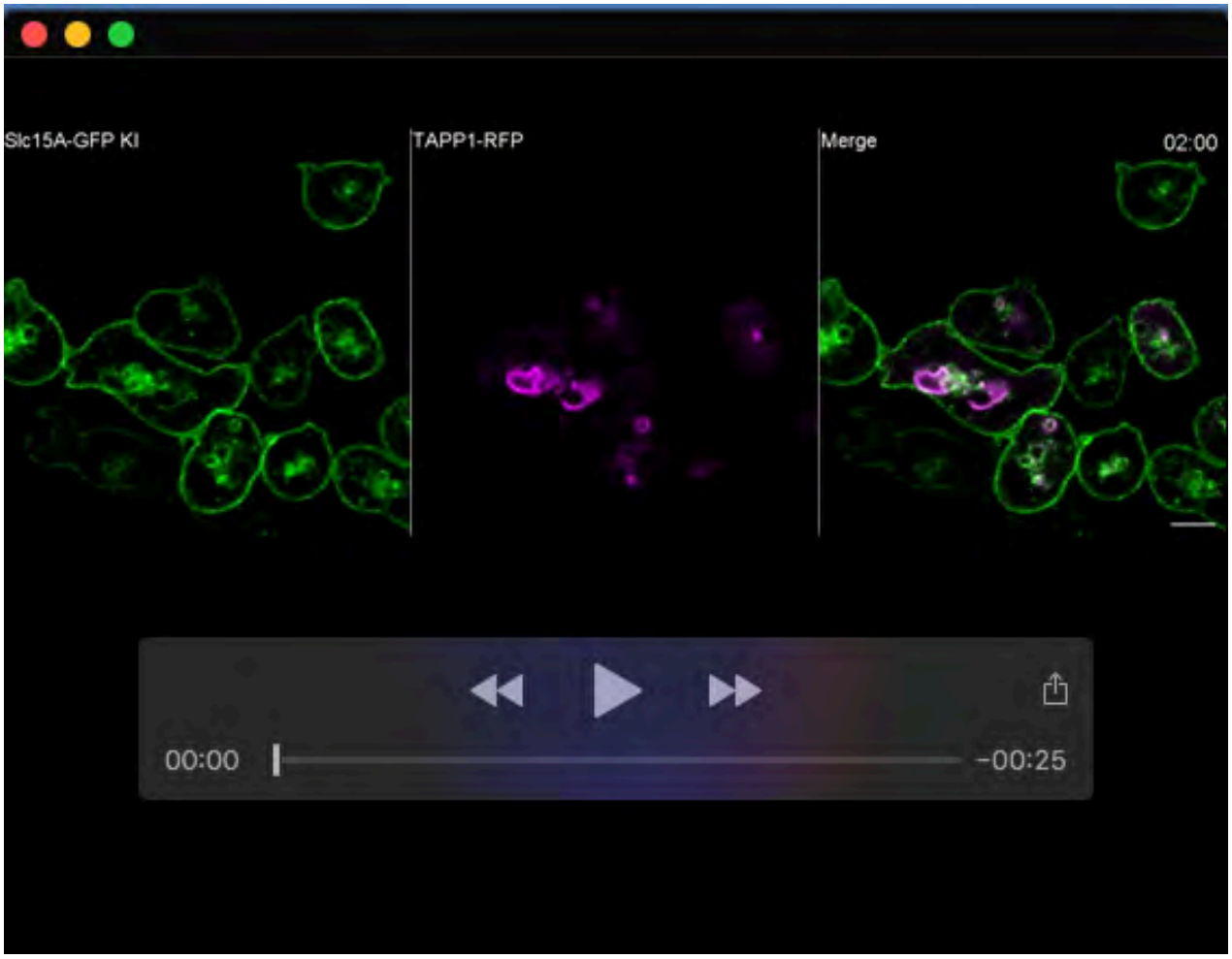

Movie 4. Colocalization of Slc15A-GFP^{KI} with the PI(3,4)P_2 sensor TAPP1-RFP. Corresponds to figure 7A. Images were captured at 15 sec per frame and played back at 6 frames per second. Scale bar, 5 µm.